Università degli Studi di Cagliari

DOTTORATO DI RICERCA

Progettazione Meccanica

Ciclo XXIII

TITOLO TESI

Statistical approach on the mechanical characterization
of AA 2XXX Friction Stir Welded butt joints
Settore/i scientifico disciplinari di afferenza
ING-IND/16

Presentata da: **Aurelio Tronci**

Coordinatore Dottorato   **prof. ing. Natalino Mandas**

Relatore   **prof. ing. Gennaro Dionoro**

Esame finale anno accademico 2009 – 2010

1. Introduction

Friction stir welding (FSW) is a solid state joining process developed at The Welding Institute of Cambridge (UK) and patented in 1991 [1]. Since its first releasing it seemed to deal in the best way with the actual industrial concern with ambient, environment and energy saving, due to its potentialities related to its ability to diminish waste of material and to avoid radiation and pollutant, toxic gas emissions usually associated to the fusion welding processes. This welding technique makes use of a non-consumable welding tool, basically constituted by a small diameter entry probe and a concentric larger diameter shoulder, both of them usually made by high strength steel. During the welding process the tool is put in rotation and plunged into the boundaries of the parts to join, until the shoulder is in intimate contact with them. The heat generated by friction between the rotating tool and the material to join promotes a local increase in temperature and softens the materials under the surface of the shoulder. At the same time the plunged rotating probe moves and mixes the softened material joining both of them in a solid state weld (fig. 1).
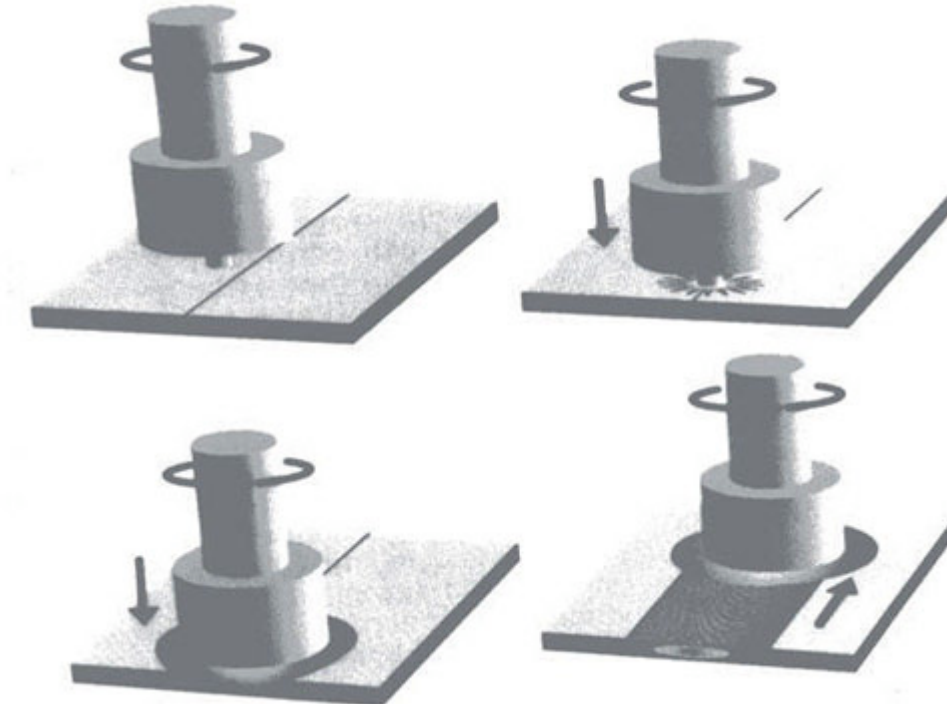

Fig.1 - Phases of FSW.

Mechanic deformation and heat generate welds that are comprised of two main zones, the thermomechanically affected zone (TMAZ) and the heat-affected zone (HAZ) (fig. 2). While the HAZ of FSW joints is given by metallurgical transformations that can be considered analogous to the ones occurring in the HAZ resulting from fusion welding processes, the TMAZ is not corresponding to the fusion zone of conventional welds, because in state of being melted the materials have been mechanically worked by plastic deformation. More detailed description of the process and the microstructure of typical FSW joints are also available in the literature [2,3].
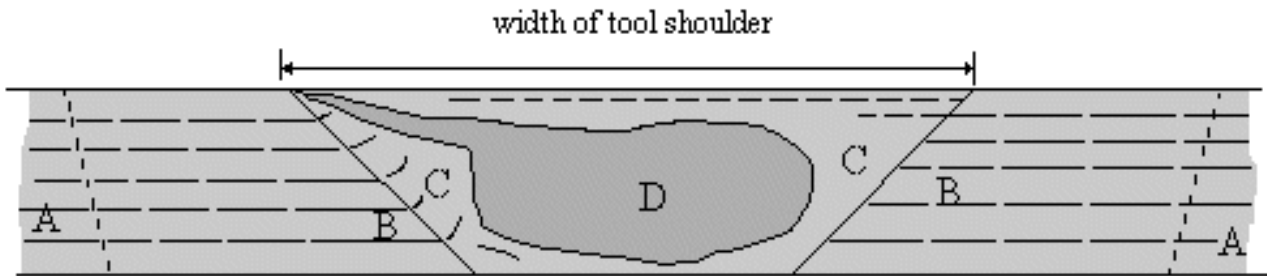
Fig. 2 - Weld zones. A Base material, B HAZ, C TMAZ and D weld nugget.

Because of the interesting features of FSW, lots of research activities have been carried out on different materials such as steel [4-7], titanium [8,9], magnesium [10,11], copper [12-14], MMC's [15,16], but the primary research and industrial interest for this process was for butt and lap joining of aluminium alloys, especially for the 2XXX, 6XXX and 7XXX series of heat treatable alloys, usually considered to be "unweldable". Among the 2XXX series, the friction stir welding of 2024 was the most studied, either in similar [17-23] and dissimilar configuration [17,23-25]. Some efforts were also spent in the study of the 2219 [26-29], 2195 [30] and 2198 [31]. In particular, FSW of AA 2198 and AA 2139, that are the alloys under investigation in this work, has found its application in the production of lightweight structures that require a high strength-to-weight ratio and good corrosion resistance [32].

If compared to other welding techniques, FSW shows advantages because of low residual stresses, low distortion and high joint strength [18,23,32,33]. Nevertheless, during this process, the tool, because of its rotational and welding speeds, exerts in-plane (horizontal) and perpendicular (vertical) forging forces on the plates to weld. The action of these forces, in addition to the effect of thermal impact, may cause the deformation of the fixture and of the welded plates, as well as influence the tool wear. Hence, a precise force control in FSW can have strong consequences and generate benefits regarding the productivity and the weld quality. Many significant settlements can be obtained keeping the welding forces at a defined level: optimization of fixturing, tool breakage prevention, tool life prediction, prediction of clamping forces, etc. Because of it, applying force control in robotised FSW would be very helpful for the increase of weld's properties.

However, to build an efficient control technique for FSW, a well-founded force prediction model needs to be developed. The development of FSW force models is not an easy task to reach, considering that it was proved that the clamping force contains static nonlinearities in function of tool rotational speed, longitudinal speed, tool plunge depth and the thermo-mechanical performance of the materials [33]. On the other side, it is also essential to have a complete control over the relevant process parameters to maximize the yield and tensile strength on which the quality of a weld is based.

Several researchers have established that an efficient use of statistical techniques allows developing an empirical methodology to incorporate a scientific approach in the FSW procedure [34-38]. Indeed, the design of experiments (DOE) was used in several papers to conduct test campaigns. The interdependence of process parameters and the development of empirical models for the prediction of tensile strength of friction stir welded joints were explored. For instance, Elangovan et al. [36] developed a mathematical model to predict the tensile strength of friction stir welded AA 6061 and optimised the process parameters to obtain maximum tensile strength, using the DOE, the response surface method and the Hooke and Jeeves algorithm. The model was developed by incorporating welding parameters and tool profiles. Balasubramanian [37] established an empirical relationship to predict the optimal FSW process parameters, to produce defect free joints starting from base material properties (yield strength, ductility and hardness).

Lakshminarayanan et al. [38], developed a response surface methodology, based on a three factors three-level central composite design with full replications, to predict the tensile strength of friction stir welded AA7039 aluminium alloy. Sarsilmaz et al. [39] performed a statistical analysis of the variance (ANOVA) over the influence of process parameters on the mechanical properties of friction stir welded AA 1050/AA 5083 couples. Therefore, the main aim of this investigation is to develop mathematical models for the prediction of both welding forces and mechanical strength (yield and tensile) of friction stir welded joints in order to optimise process parameters and joint's mechanical performances.

2. Materials and experimental system.

2.1 Materials

The material under investigation was supplied in 3.2 mm thick rolled sheets of AA 2198 T351 and AA 2139 T851 aluminum alloys and were cut into the required size (200 mm x 100 mm) by power hacksaw cutting. Chemical composition and main mechanical properties of the alloys are listed in table 1 and 2.

	Si %	Fe %	Cu %	Mn %	Mg %	Cr %	Zn %	Zr %	Li %	Ag %	Ti ppm
AA2139 T851	0.04	0.06	5.07	0.29	0.43	-	-	0.014	-	0.10	510
AA2198 T351	0.08	0.10	3.50	0.50	0.80	0.05	0.35	0.18	1.10	0.50	-

Tab. 1 - Alloying elements in AA 2139 and AA 2198.

	UTS [MPa]	YS [MPa]	E [GPa]	Elongation %
AA2139	451	402	70	14.3
AA2198	370	275	74	15

Tab. 2 - Measured tensile mechanical properties of AA 2139 T851 and AA 2198 T351.

The AA 2139 alloy has a modified precipitation sequence due to artificial ageing. The addition of Ag leads to enhanced ageing kinetics and to a significant increase in strength, due to the formation of a fine and uniform dispersion of Ω phase precipitates on {111} planes of the aluminum matrix [14]. Plate-like precipitates on these planes have a greater impact on strengthening than precipitates on the other planes. This precipitation mechanism becomes the dominant one with respect to the precipitation of θ ' (Al_2Cu) phase on {100} planes that is usually observed in Al–Cu–Mg alloys. The fine and uniform distribution of the new Ω precipitates, considering its good thermal stability, and the optimum balance of them with the θ' precipitates, leads the AA 2139 alloy to have superior strength and creep resistance at temperature up to 250 °C. Moreover, these alloys have less grain boundary precipitation, and therefore retain most of their toughness after age hardening, and are less susceptible to intergranular fracture. The structure and morphology of the Ω and θ' precipitates after intense plastic deformation suggest that multiple dislocations interact with the Ω precipitates. No pile-ups appear, and the mechanism of multiple shear-cuttings of_is operative at high strain rate [15]. The T851 temper condition corresponds to solution heat treatment in the range of 480–520 °C for 10 min, cold work at a strain range of 2–4 per cent followed by artificial aging in the range of 150–180 °C for 16 h.

The AA 2198 is an Al-Cu alloy characterized by the consistent presence of Li, which is the lightest element (with specific mass of 0.536 ton/m^3) among the components used for

alloying commercial aluminum alloys. The introduction of 1% Li decreases the specific weight of aluminum alloys by 3% and simultaneously raises the modulus of elasticity by 6%. In addition to the enhanced rigidity, Al – Li alloys possess high strength parameters and resistance to fatigue loads in combination with good corrosion resistance and satisfactory weldability.

2.2 Experimental system.

The experimental system used was compound by a CNC machine, a specific friction stir welding made tool and a data acquisition system.

The machine used to make the friction stir welded joints was a five axes DMG CNC machine with a 0 x 600 x 600 (x / y / z) workspace, instrumented with a Kistler three-axis dynamic force load cell connected to a signal amplifier, in order to record forces along both the plunging direction (Fz) and the welding direction (Fx) for all the produced welds. In addition, during the welding process a thermal analysis was performed using a Nec TH 7800 thermal-camera. The Cr-Mo steel welding tool (fig.1) had a shoulder radius of 12 mm while the unthreaded pin was 4 mm in diameter and 3 mm long. The forging action of the tool shoulder was enhanced by a tool tilt angle of 2°.

A National Instruments data acquisition system was used for the force signal acquisition, including NI USB 6251 with 1.25 MS/s scan rate board. A sampling rate of 50 Hz was employed in all experimental studies.
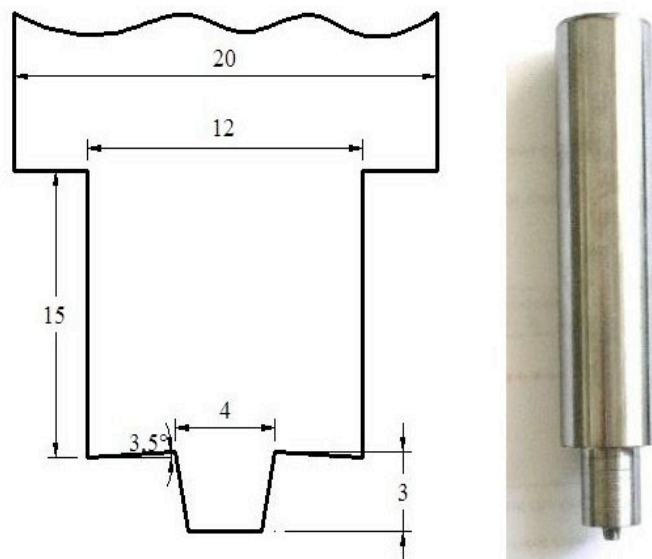

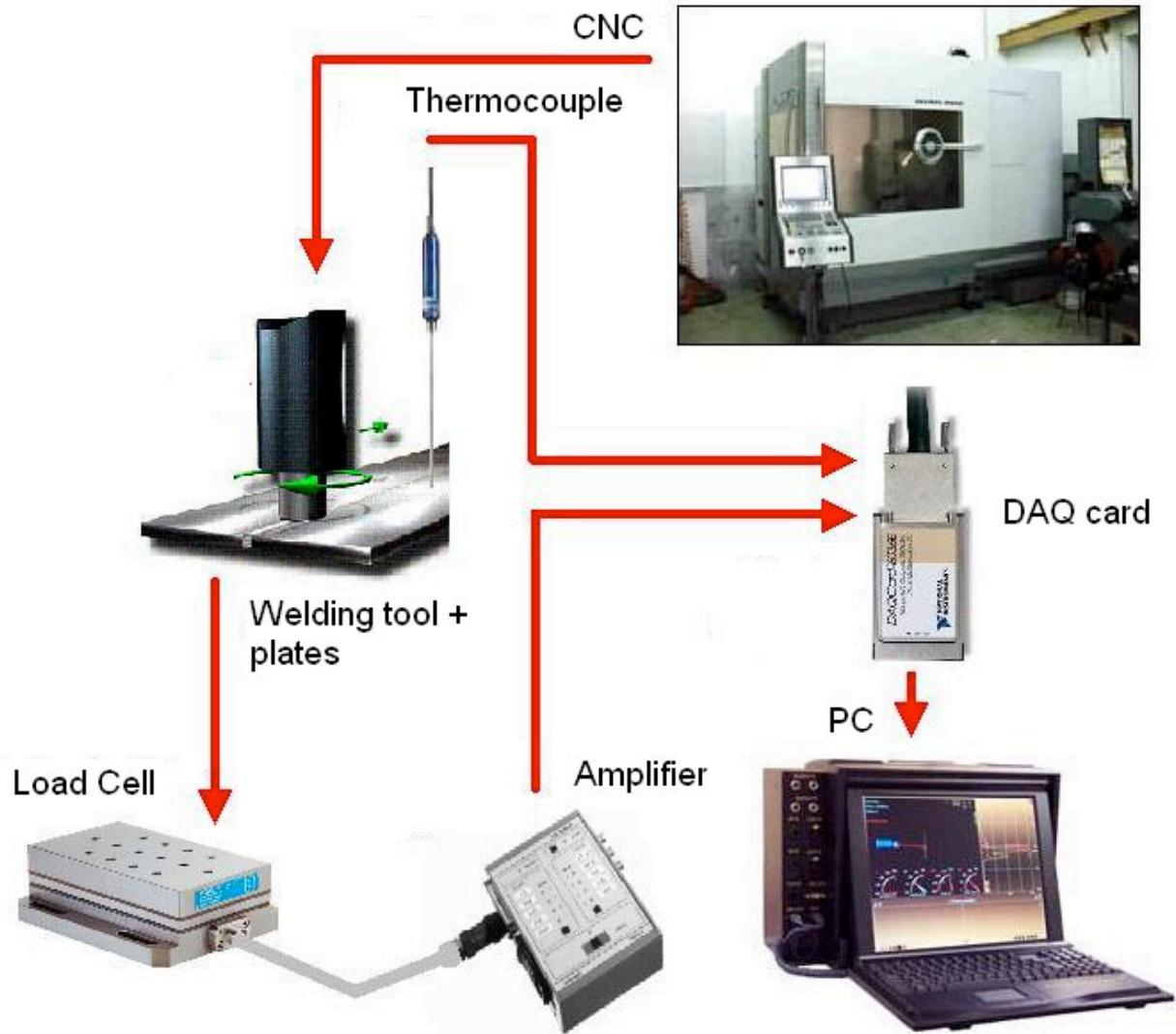fig. 3 Welding tool geometrical features (all dimensions in mm).

Fig. 4 - Experimental system.

In order to realize welding on CNC machine, it was necessary to develop a part-program suitable for the controller. It was divided in two parts, where the first one performs the tool approach into the material and the second one the tool progress along the welding direction. The first part was always the same for each test, with feed rate = 5 mm/min along z axis, while the second part has different weld rate, feed rate along x axis and penetration depth for each test.

Load cell was set along 3 coordinate axes. Five different weights were used to verify the linear characteristic of the force sensor. Figure 3 shows the linear characteristic of z and x axes for 1, 5 and 10 kN range.
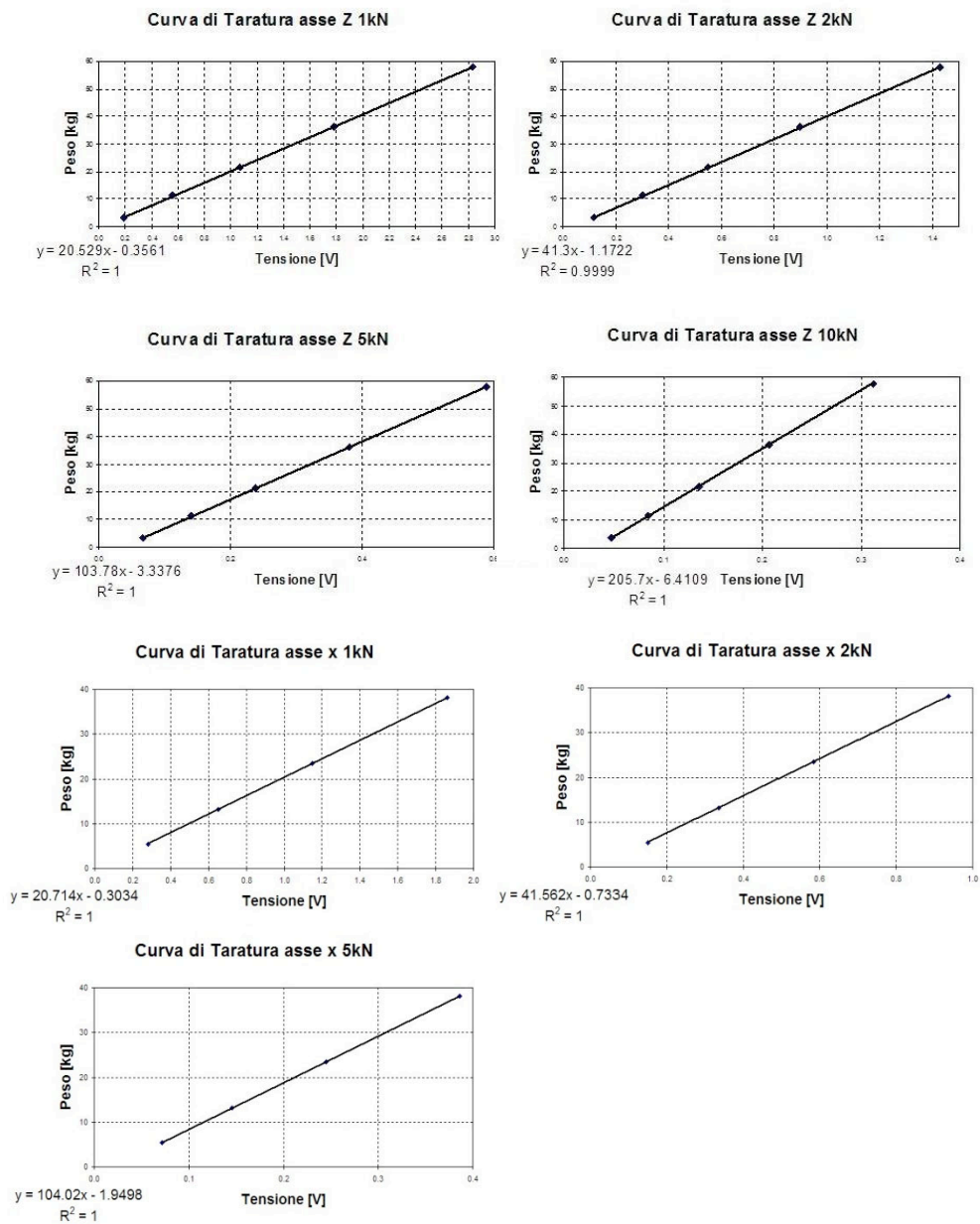
Fig.5 - Linear characteristic of the load cell.

3. Mechanical characterization.

Static tensile tests were performed on samples consisting of three valid specimens from each weld. Tests were carried out on specimens having the weld bead perpendicular to loading direction and according to ASTM B557M on a Zwick /Z 100 kN (figs. 6-7-8).
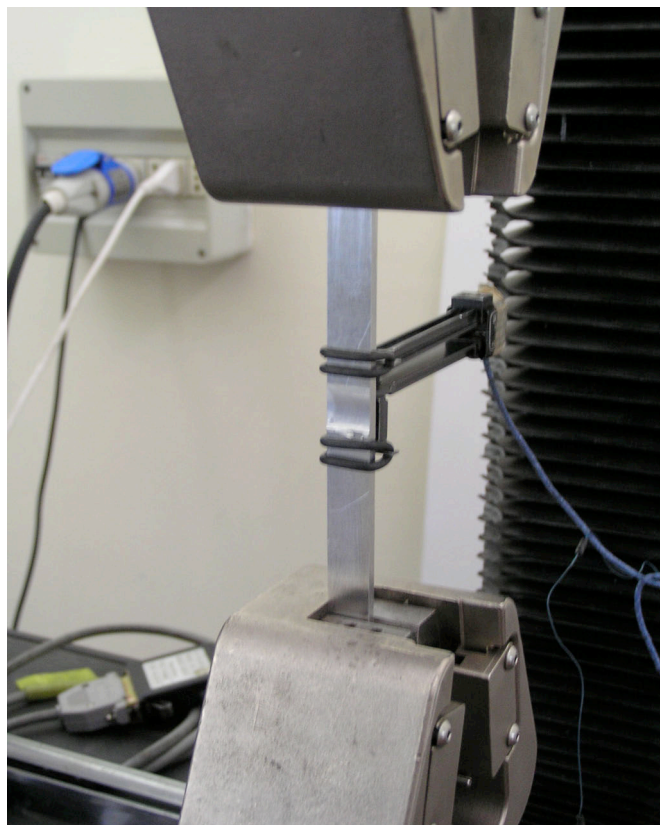

Fig. 6 - Tensile test machine Zwick /Z 100 kN.

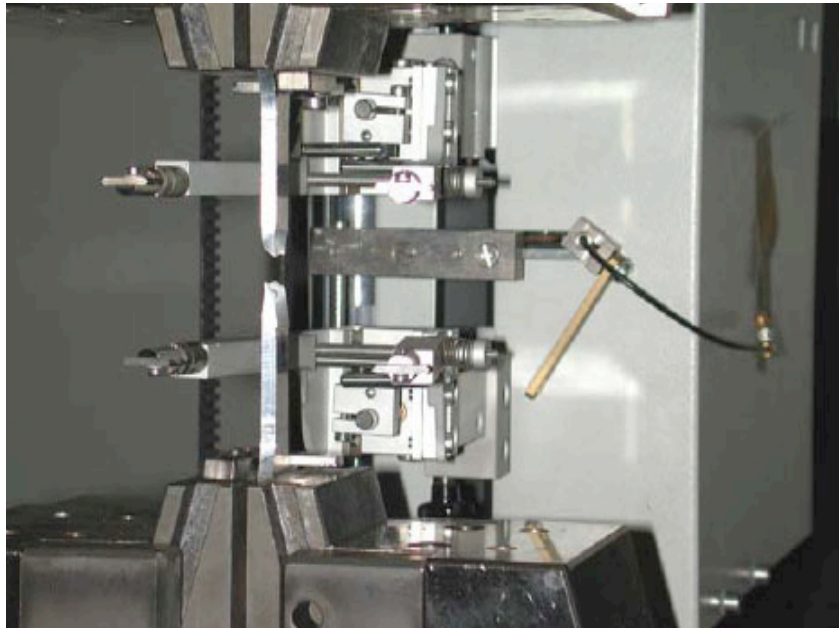
Fig. 7 - Particular of the sample.

Fig. 8 - Particular of the specimen instrumented with an extensometer.

4. Design of experiments.

4.1 General

The goal of any experimental activity is to get the maximum information about a system with the minimum number of well designed experiments. An experimental program recognizes the major "factors" that affect the outcome of the experiment. The factors may be identified by looking at all the quantities that may affect the outcome of the experiment. The most important among these may be identified using a few exploratory experiments or from past experience or based on some underlying theory or hypothesis. The next thing one has to do is to choose the number of levels for each of the factors. The data will be gathered for these values of the factors by performing the experiments by maintaining the levels at these values. Suppose we know that the phenomena being studied is affected by the pressure maintained within the apparatus during the experiment. We may identify the smallest and the largest possible values for the pressure based on experience, capability of the apparatus to withstand the pressure and so on. Even though the pressure may be varied "continuously" between these limits, it is seldom necessary to do so. One may choose a few values within the identified range of the pressure. These will then be referred to as the levels.

Experiments repeated with a particular set of levels for all the factors constitute replicate experiments. Statistical validation and repeatability concerns are answered by such replicate data.

In summary an experimental program should address the following issues:

- Is it a single quantity that is being estimated or is it a trend involving more than one quantity that is being investigated?
- Is the trend linear or non-linear?
- How different are the influence coefficients?
- What does dimensional analysis indicate?
- Can we identify dimensionless groups that influence the quantity or quantities being measured

- How many experiments do we need to perform?
- Do the factors have independent effect on the outcome of the experiment?
- Do the factors interact to produce a net effect on the behavior of the system?

4.2 Full factorial design

A full factorial design of experiments consists of the following:

- Vary one factor at a time
- Perform experiments for all levels of all factors
- Hence perform a large number of experiments that are needed!
- All interactions are captured

Consider a simple design for the following case:

Let the number of factors = k
Let the number of levels for the ith factor = n_i

The total number of experiments (n) that need to be performed is

$$n = \prod_{i=1}^{k} n_i$$

and number of levels is 3 for each of the factors the total number of experiments to be performed in a full factorial design is $3^5 = 243$.

2k factorial design:

Consider a simple example of a 2k factorial design. Each of the k factors is assigned only two levels. The levels are usually High = 1 and Low = -1. Such a scheme is useful as a preliminary experimental program before a more ambitious study is undertaken. The outcome of the 2k factorial experiment will help identify the relative importance of factors and also will offer some knowledge about the interaction effects. Let us take a simple case where the number of factors is 2. Let these factors be xa and xb. The number of experiments that may be performed is 4 corresponding to the following combinations:

Experiment	xa	xb
1	+1	+1
2	+1	-1
3	-1	+1
4	-1	-1

Tab.3 - Full factorial design.

Let us represent the outcome of each experiment to be a quantity y. Thus **y1** will represent the outcome of experiment number 1 with both factors having their "High" values, **y2** will represent the outcome of the experiment number 2 with the factor A having the "Low" value and the factor B having the "High" value and so on. The outcome of the experiments may be represented as the following matrix:

Experiment	xa	xb	y
1	+1	+1	y1
2	+1	-1	y2
3	-1	+1	y3
4	-1	-1	y4

Tab. 4 - Full factorial design response.

A simple regression model that may be used can have up to four parameters. Thus we may represent the regression equation as

$$y = p_0 + p_a x_a + p_b x_b + p_{ab} x_a x_b$$

The p's are the parameters that are determined by using the **"outcome"** matrix by the simultaneous solution of the following four equations:

$$\begin{cases} p_0 + p_a + p_b + p_{ab} = y_1 \\ p_0 - p_a + p_b - p_{ab} = y_2 \\ p_0 - p_a - p_b - p_{ab} = y_3 \\ p_0 - p_a - p_b + p_{ab} = y_4 \end{cases}$$
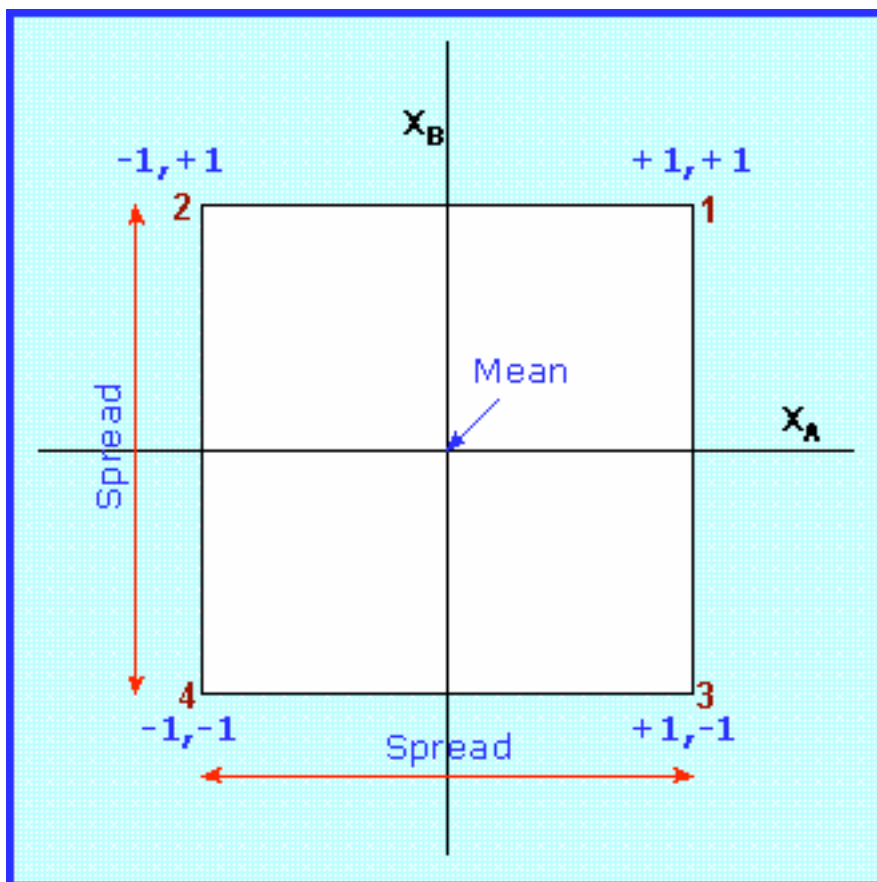

Fig. 9 - Full factorial design interpretation.

It is easily seen that the parameter p_0 is simply the mean value of y that is obtained by putting $x_a = x_b = 0$ corresponding to the mean values for the factors. The system of equations expresses the fact that the outcome may be interpreted as shown in fig. 9. It is thus seen that the values of y- p_0 at the corners of the square indicate the deviations from the mean value and hence the mean of the square of these deviations (we may divide the sum of the squares with the number of degrees of freedom = 3) is the variance of the sample data collected in the experiment. The influence of the factors may then be gauged by the contribution of each term to the variance.

5. Experimental study.

5.1 AA 2139 T851
The Design of Experiment (DOE) technique was used to gather information about the influence of different process parameters on the mechanical characteristics of the joints and, finally, to determine the best parameters combination to improve the performance of the welds at the same time [rif.].
A full factorial 3^3 design with 4 times replied central point was realized. This experimental strategy contemplates random tests execution to avoid that systematic errors could involve the experiment results. Process parameters were: tilt angle, plunge thickness, rotational speed, welding rate and the relative position of the specimens to run-in. The first two were fix factors, were set at 2° and all thicknesses of the rolled plates. The rotational speed welding rate and plunge depth were classified as range value, as are variable factors.

Sample	N [RPM]	Level	V [mm / min]	Level	Position [mm]	Level
			Factors			
1	1400	0	175	0	0.10	0
2	800	-1	300	+1	0.10	0
3	2000	+1	175	0	0.13	+1
4	800	-1	175	0	0.13	+1
5	1400	0	175	0	0.10	0
6	1400	0	175	0	0.10	0
7	1400	0	300	+1	0.13	+1
8	1400	0	175	0	0.10	+1
9	2000	+1	175	0	0.07	-1
10	1400	0	50	-1	0.07	-1
11	800	-1	50	-1	0.10	0
12	2000	+1	50	-1	0.10	0
13	1400	0	50	-1	0.13	+1
14	800	-1	175	0	0.07	-1
15	2000	+1	300	+1	0.10	0
16	1400	0	300	+1	0.07	-1

Tab.5 – Working parameters experimental set

The two welding plates were fixed on machining board, the three working parameters were set in input to part program as experimental plan. Sensor force signal acquisition software and part program started at the same time.

5.1.1 Macro and Micro Structural characterization

The macro and micro-structural characterization were aimed to investigate the evolution of the microstructure and the resulting mechanical properties. Standard metallographic techniques in agreement with the standard test methods ASTM-E3 were applied for the characterization of microstructures. After etching by Keller's reagent (tab.6) each specimen was macro and micro examined with light microscope in order to identify the extension of each typical region associated to the FSW process: the nugget zone (NZ), the thermo-mechanically affected zone (TMAZ), the heat-affected zone (HAZ), and the base material (BM). The macro-structural examinations were made with a magnification up to 5×. The micrographic analysis was made with a magnification up to 1250×.

Reagent	HF ml	HCl ml	HNO$_3$ ml	H$_2$O ml
Keller's	2	3	5	190

Tab. 6 - Chemical composition of Keller's reagent.

Micro-hardness measurements were performed in the cross sections of all the welds in agreement with the standard ASTM E384 using a Vickers indenter having a mass of 0.5 kg. In order to map the micro-hardness each joint, the whole cross section has been divided in a grid of 65 areas as highlighted in Fig. 10.
The micro-structural characterization was split in two different phases: the defect analysis and the mean grain size measurements. The defect analysis allowed identifying the morphology of the weld defects, their comparison with the results of the mechanical tests allowed to highlight the influence of defects on the joint strength. Two kinds of defects have been observed: the kissing bond and the tunnel; they are depicted, respectively, in Figs 11 and 12. The mean grain dimension mapping has been made using the same grid of the micro-hardness.

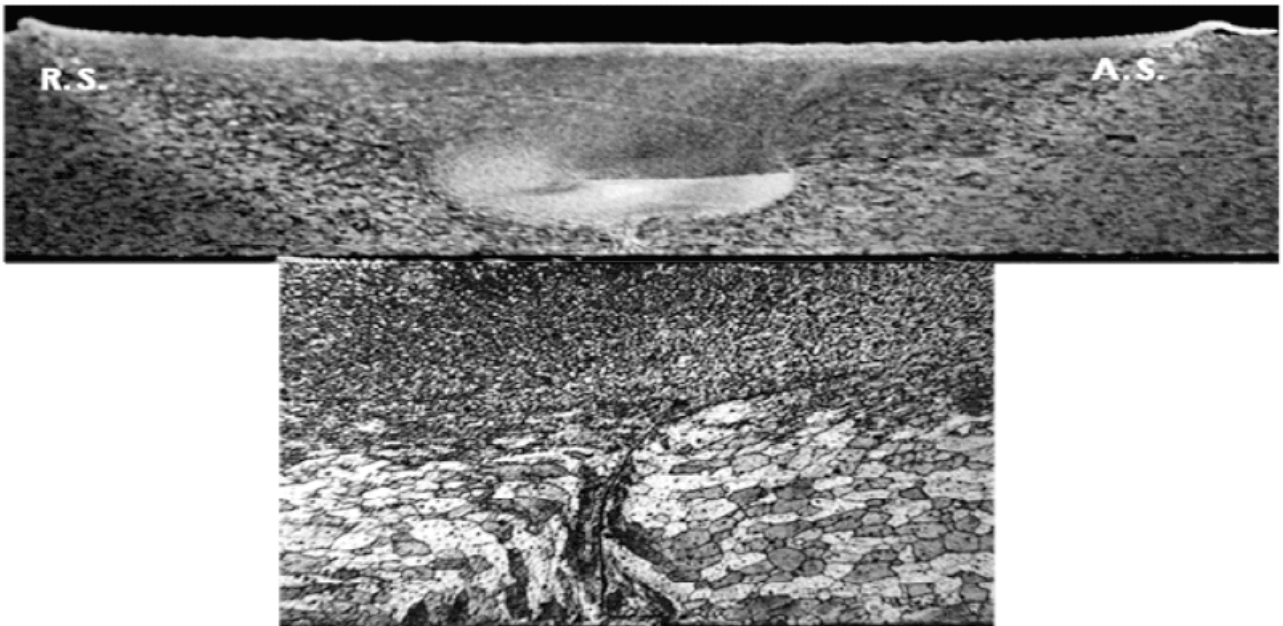Fig. 10 - Grid of mean grain and micro-hardness measurements.
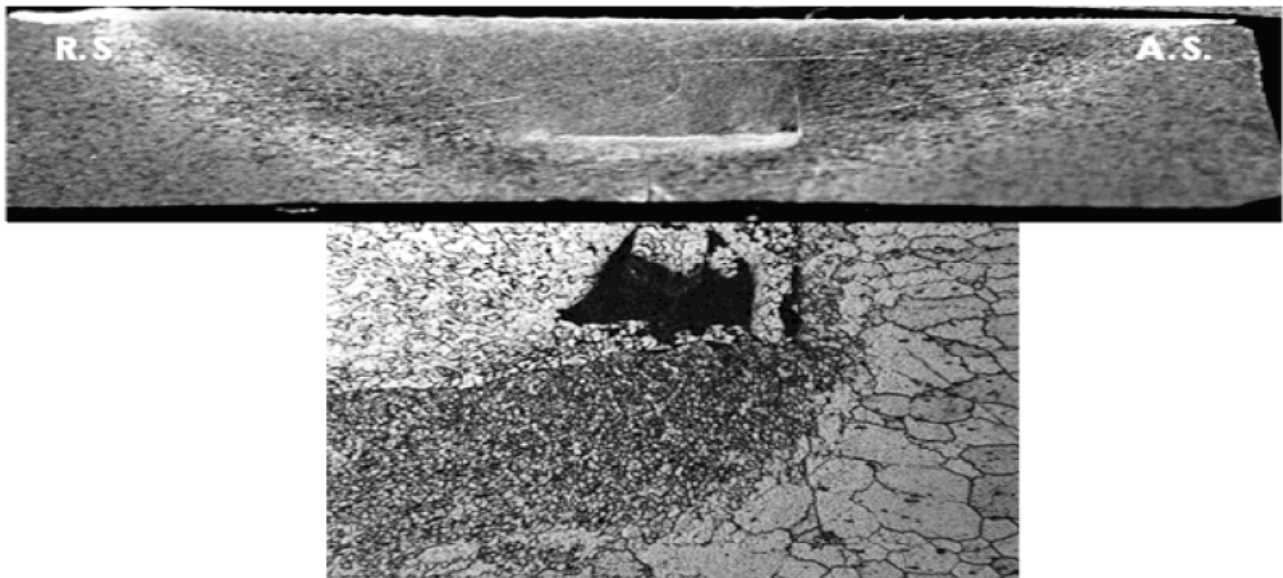
Fig. 10 - Kissing bond defect.

Fig. 11 - Tunnel defect.

5.1.2 Obtained results.

5.1.2-a. Forces and temperatures.

Test Number	Z Axis			Y Axis			Temperature
	Fmean	Fmax	Fmin	Fmean	Fmax	Fmin	
1	11500	11700	11500	1660	1890	1230	480
2	13600	13600	13500	1030	1250	790	340
3	8200	9300	7300	1020	1900	140	510
4	12800	12900	12800	920	1130	586	380
5	11300	11600	11000	1760	1910	1580	480
6	11600	12000	11100	1640	1870	1290	480
7	12600	13600	10200	2050	2240	1730	450
8	11200	11700	10400	1600	1820	1300	480
9	7500	8700	6000	1000	2050	193	490
10	8600	8800	8300	850	1060	610	510
11	9000	9100	8700	780	920	610	500
12	4600	5800	3400	350	1050	150	570
13	6300	6300	6300	940	1130	730	520
14	13600	13600	13600	1040	1320	780	380
15	11000	11800	9200	1700	2220	473	450
16	13600	13600	13600	1990	2270	1610	390

Tab. 7 - Resume of the Z, X axis forces and measured temperatures.

Table 7 shows post-process analysis force sensor signals along the *x*- and *z*-axis. For every produced weld, the signal of forces acting on the tool along the *x*- and *z*-axis have been recorded, as reported, for example, in Fig. 12.
By analysis of the forces, can be noticed two transient zones and one regime condition zone for force along z axis, while one transient zone and one regime condition zone for force along x axis.
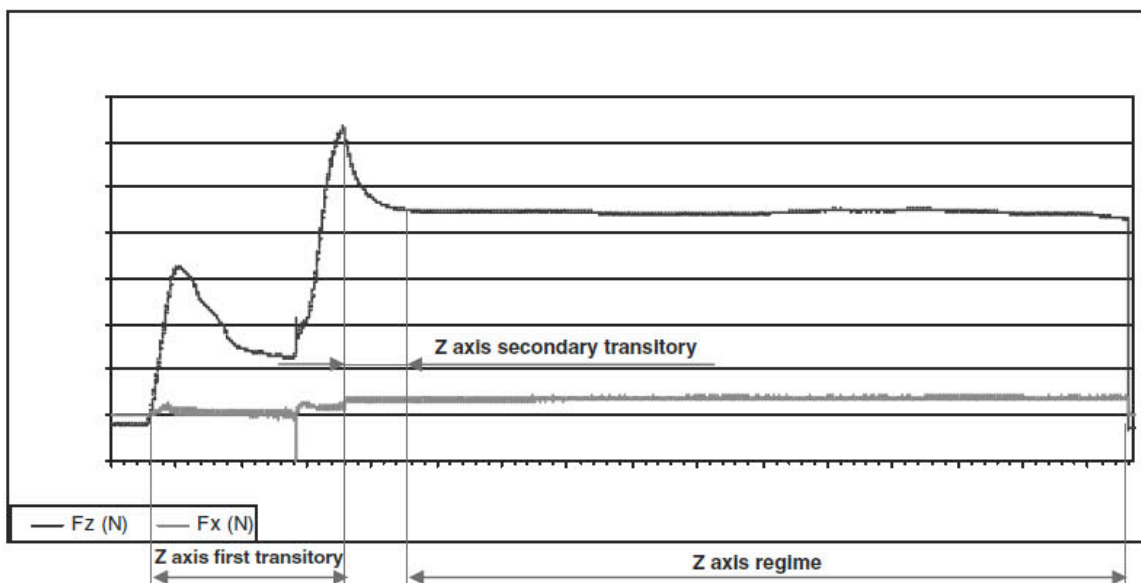

Fig. 12 - Force signals recorded during test number 5.

Analyzing the force signal along z axis, we can achieve the following observations: a zone of first transient when the tool gets into the material along z axis and a zone of second transient when the tool starts to advance along x axis can be noted. In the first transient (only getting in z direction) can be seen a peak where Fz rapidly increases because tool pin gets into the material and thermal regime conditions aren't so high. The yield stress is still high so forces quickly increase. In the first peak, force values depend by rotational speed (N). So, increasing N, first peak max force value decreases, because a higher rotational speed, correspond higher thermal value and lower deformation resistance.

After material reaches some plasticity degree, Fz decreases for some time, then rapidly increases again when the tool shoulder gets into the material. Because the shoulder is larger than the pin, it affects much more opposing material, creating greater resistance so that Fz rapidly increases. In Tab.4 shows the average values of Fz peak when the tool shoulder get into the material.

In every test the first transient period is not always the same due to the same tool feed rate along z axis (5 mm/min) but different plunge depth to reach. When the tool reaches the desired penetration depth it begins to advance along x axis (welding line). At this moment the secondary transient of z axis starts. It lasts for a different period according to process parameters (different feed rate along x axis). The material soon reaches a regime condition and Fz stabilizes.

Analyzing the force signal along x axis the following observations can be carried out. While tool gets into the material Fx = 0 (stop tool along x axis). When tool starts to move along x axis, Fx increases and quickly reaches a regime condition.

Sometimes there is no or negligible transient zone in comparison with the steady state. Fx is essentially governed by feed resistance, including friction resistance, opposed by the material. During all the tests Fz has never been higher than 12 000 N, and Fx has never been higher than 2000 N. Medium, maximum, and minimum values, along both axes, were measured for regime conditions.

Many photos were taken with the thermal-camera (fig. 13 a-b). Therefore, it was possible to get a temperature map around the tool – welding line contact point. The acquisition rate of the thermal images is constant, and so the higher the v_a the lower the number of available thermal images. During the realization of the weld-test 10 (see Table 7) the temperature immediately achieved at the welding start was approximately 210 °C; during the welding it increased to reach the maximum value of 510 °C. Analysing temperature values reported in Fig. 14 it can be appreciated how the lower pitch v_a/ω the higher temperature value.
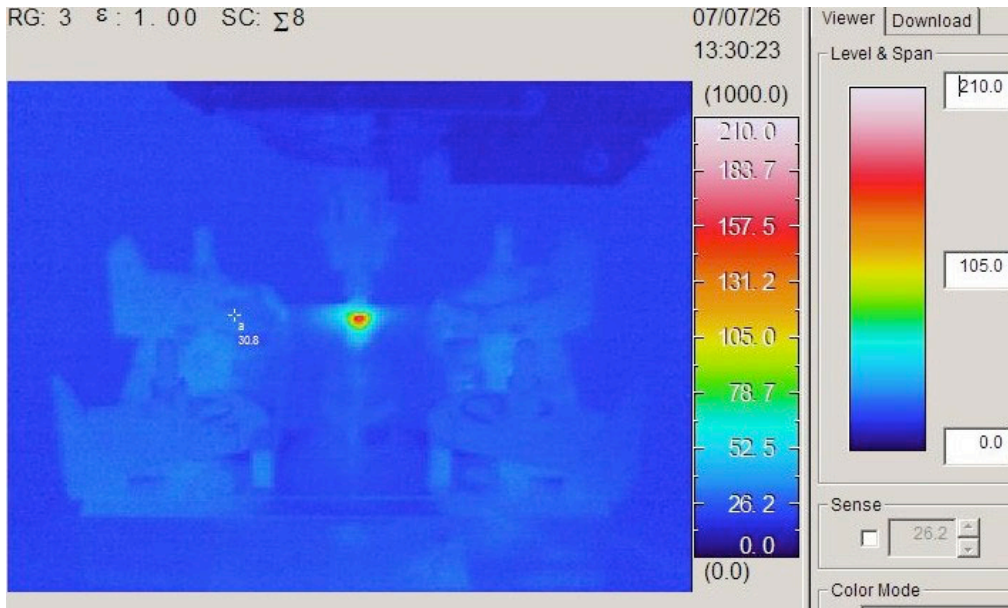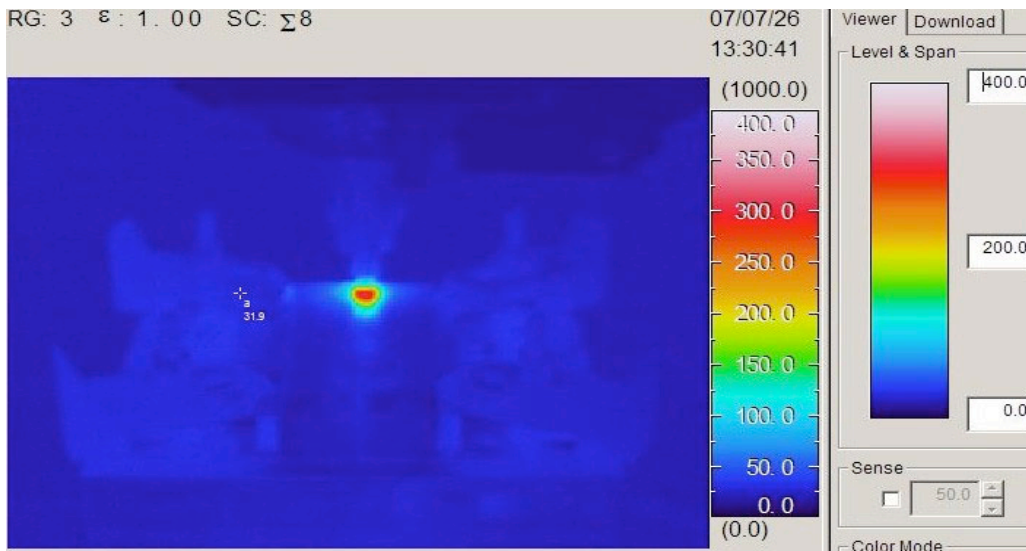
Fig. 13 a-b Thermal pictures taken during two different tests (8 and 12).
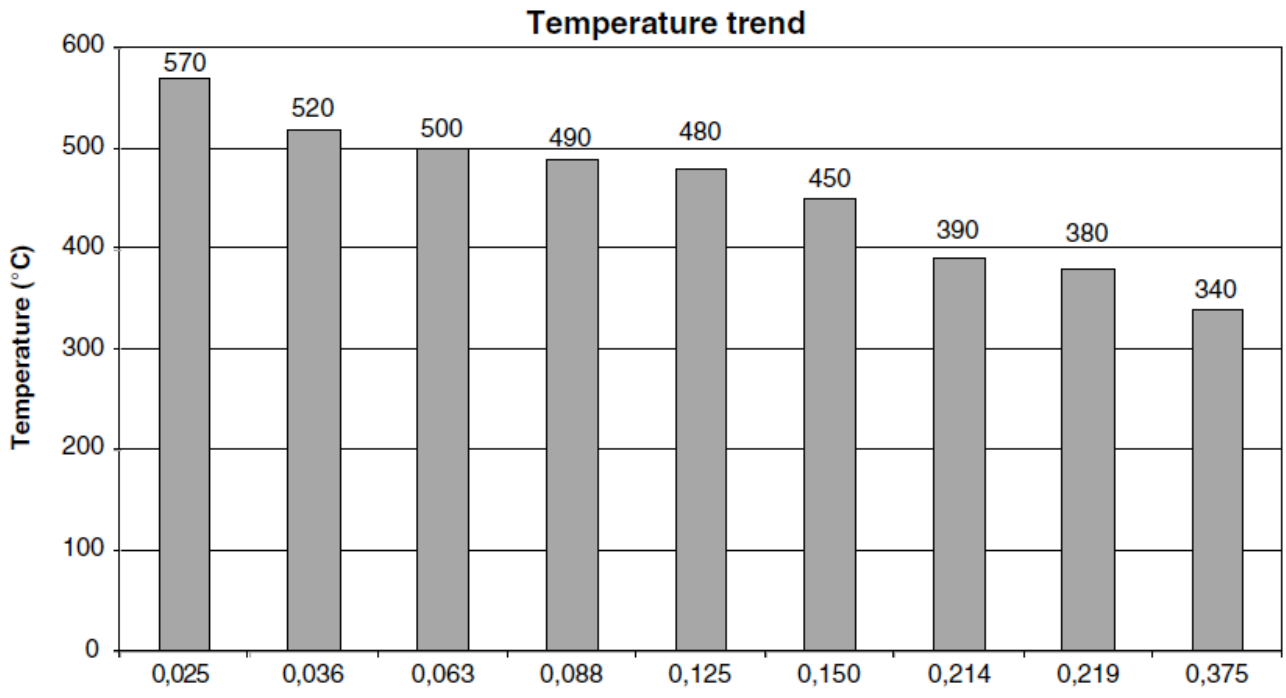
Fig. 14 - Temperature trend vs weld pitch.

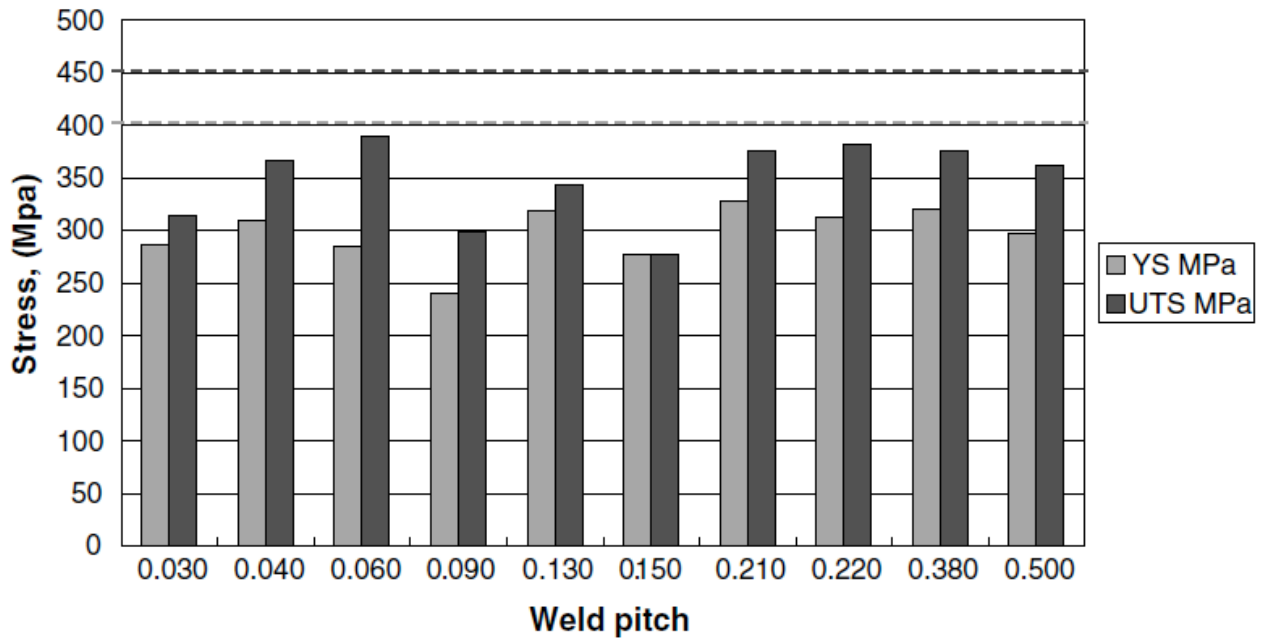## 5.1.2-b Tensile tests and statistical analysis.

Fig. 15 - UTS and YS vs weld pitch.

Results of static tensile tests are shown in Fig. 15, where both yield strength (YS) and ultimate tensile strength (UTS) attained by joints are reported versus weld pitch; dotted lines represent values attained by the parent material. Apparently no significant trends can be appreciated, but splitting the influence of welding and angular speed (Fig. 16) it is easy to see how UTS decreases as angular speed increases while it remains quite constant as welding speed increases. YS, on the contrary, varies with no appreciable trend, with the exception of a light increase as welding speed increases. In any case, however, the best joints achieve a recovery of the mechanical properties, with respect to parent alloy close to 81 per cent of YS and 86 per cent of UTS. Efficiencies achieved, summarized in Table 9, are comparable with those achieved for FSW joints of AA6056 T6 [47, 48], AA6082 T6 [49], and greater than those achieved in AA2024 [50]. Now focusing attention on estimated response surface provided by data statistical analysis, trends of joints efficiency as a function of welding parameters are shown in Fig. 17. It is evident how the best UTS and the best YS values are not achieved with the same set of the parameters. The three-dimensional (3D)-plots in Figs 17(a) and (b) show that the UTS values attain a maximum when the weld is made with the highest p and the lowest ω, the v_a influence being practically negligible. Figures 17(c) and (d) refer to the YS.
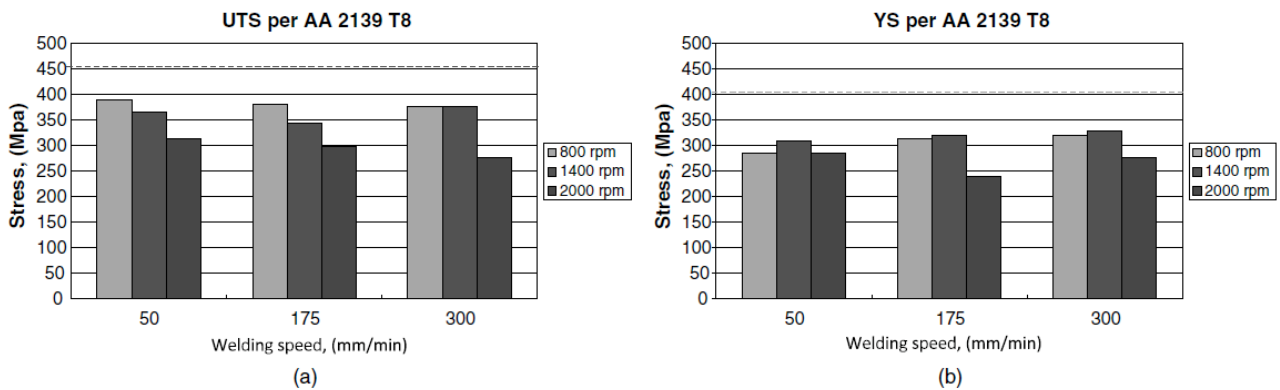
fig. 16 Influence of welding and rotating speed on UTS (a) and YS (b).

η [%]		ω [RPM]		
		800	1400	2000
v_a [mm/min]	50	86.3	81.2	69.7
	175	84.6	76.0	66.2
	300	83.3	83.5	61.5
v_a [mm/min]	50	70.8	77.0	71.1
	175	78.0	79.5	59.8
	300	79.9	81.8	69.0

Tab. 9 Efficiencies achieved for UTS and YS

This reaches the maximum at intermediate values of both angular and welding speed among the investigated ones; the shape attained by surfaces plotted in Figs 17(b) and (d) allows one to predict an appreciable interaction effect of angular speed and plunging depth, this is evident especially in Fig. 17(b). The implementation of a DOE allows recognizing the parameters affecting the process. The results of the ANOVA carried out for UTS are shown in Table 10; a regression analysis is shown in Fig. 18(a) (Pareto Chart). The UTS is strongly influenced by ω and weakly influenced by p; what's more it is not negligible their interaction. The soundness of the ANOVA is supported by residue analysis, shown in Fig. 18(b), because they have a mean equal to zero and a quite normal distribution. The influence of main parameters is shown in Fig. 19(a): it is evident that the variance induced by ω is higher than that of the other factors. On the basis of these results, it could also be possible to choose the appropriate welding parameters in order to maximize the UTS. The interaction plot in Fig. 19(b) shows the effect of the interaction between ω and p. The maximum UTS values have been achieved by those joints made with low rotational speed. Subsequently, an optimization of the regression model allowed providing a numerical expression containing only those factors having a high influence on the system

$$\text{UTS} = 672 - 0.069\,\omega - 4479p + 14530p^2 + 1.238\,\omega p \quad (1)$$

The ANOVA carried out on the YS and regression analysis in Fig. 20 show a high influence of both ω and p. It is particularly important in the interaction ω–p, likely it was observed in the previous case regarding the UTS, while ω has a significant incidence with

a quadratic trend rather than simply linear trend. The study of the residues confirms the soundness of the performed analysis. The main effect plot in Fig. 21(a) shows the influence of non-linear angular speed, as well as that of the welding speed. The last, even if not very significant, will appear in the numerical expression of the optimized model in order to ensure the greatest possible accuracy. For the YS too (Fig. 21(b)), the interactions of p with other parameters play a significant role. Through the representation of the response surface (Fig. 16), it is possible to see that, with the realized experimental plan, one is able to find a maximum of the YS, which is attained by using intermediate values of the both ω and va and with minimum p. In this case, the numerical optimization of the model led to the following expression

$$YS = 355 + 0.412v_a - 1525p - 0.0000537\omega^2 - 0.00101\,v_a{}^2 + 1.347\omega p \quad (2)$$

The ANOVA analysis of the previous paragraphs showed that the conditions to achieve the maximum UTS do not match with those permitting to achieve the maximum of the YS. The above-mentioned data are summarized in the Table 11. All mechanical properties are strongly influenced by the microstructure produced by the welding: grains size and shape and typology, dimensions and shape of precipitates. These features, in turn, are directly influenced by the heat flow and plastic deformation experienced by the material, which depend on the parameters adopted.
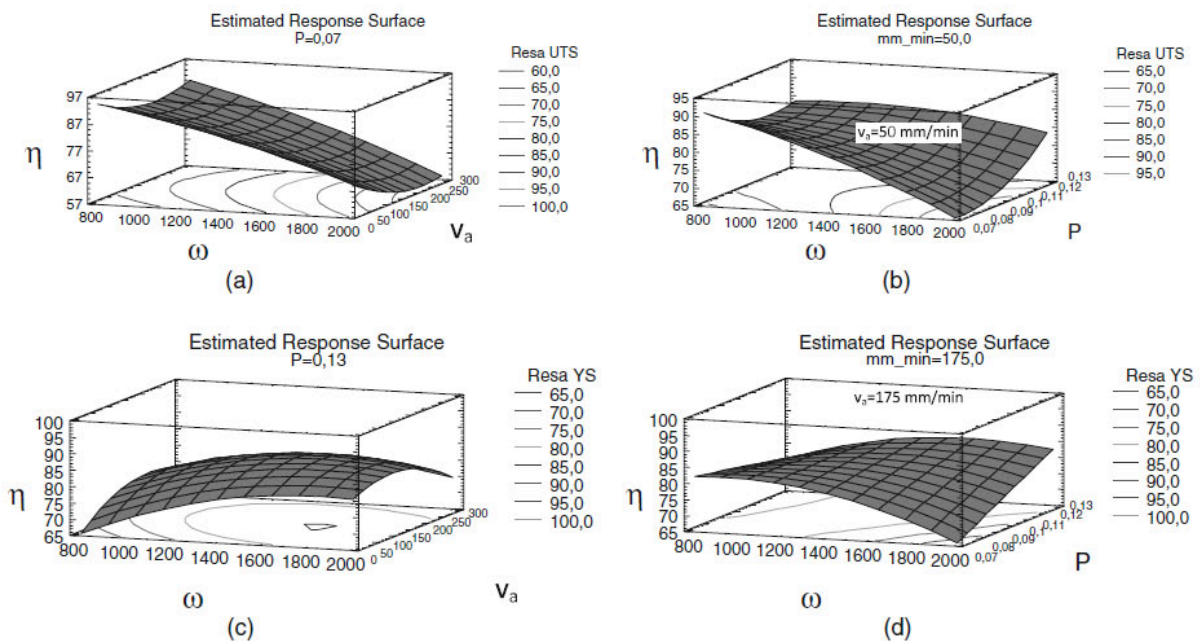

Fig. 17 - Performances of UTS (η) (a) as a function of ω and va and (b) as a function of ω and p; performances of YS (c) as a function of ω and va and (d) as a function of ω and p.

```
The analysis was done using coded units.
Estimated Regression Coefficients for Ultimate Strength

Term          Coef  SE Coef      T      P

Constant   340,921   11,761  28,987  0,000
Block        9,904    4,884   2,028  0,058
RPM        -40,850    6,552  -6,235  0,000
V           -3,281    6,552  -0,501  0,623
P           12,331    6,552   1,882  0,076
RPM*RPM    -13,985    9,949  -1,406  0,177
V*V         12,252    9,949   1,232  0,234
P*P         13,077    9,949   1,314  0,205
RPM*V       -5,763    9,266  -0,622  0,542
RPM*P       22,288    9,266   2,405  0,027
V*P          5,375    9,266   0,580  0,569


S = 26,21   R-Sq = 76,7%   R-Sq(adj) = 63,8%

Analysis of Variance for Ultimate Strength

Source          DF  Seq SS  Adj SS  Adj MS      F      P
Blocks           1    2967    2825  2825,1   4,11  0,058
Regression       9   37801   37801  4200,1   6,12  0,001
  Linear         3   29305   29305  9768,3  14,22  0,000
  Square         3    4026    4026  1342,0   1,95  0,157
  Interaction    3    4471    4471  1490,2   2,17  0,127
Residual Error  18   12363   12363   686,9
  Lack-of-Fit   15    9664    9664   644,2   0,72  0,718
  Pure Error     3    2700    2700   899,9

Total           28   53131


Unusual Observations for Ultimate Strength
                Ultimate
Obs  StdOrder  Strength      Fit  SE Fit  Residual  St Resid
 11        11   345,600  386,392  16,776   -40,792     -2,03 R

R denotes an observation with a large standardized residual.
Estimated Regression Coefficients for Ultimate Strength using data in uncoded units

Term            Coef
Constant      672,506
Block         9,90417
RPM        -0,0696815
V           -0,336463
P           -4479,28
RPM*RPM  -3,88484E-05
V*V        0,000784133
P*P          14530,1
RPM*V    -7,68333E-05
RPM*P        1,23819
V*P          1,43333
```
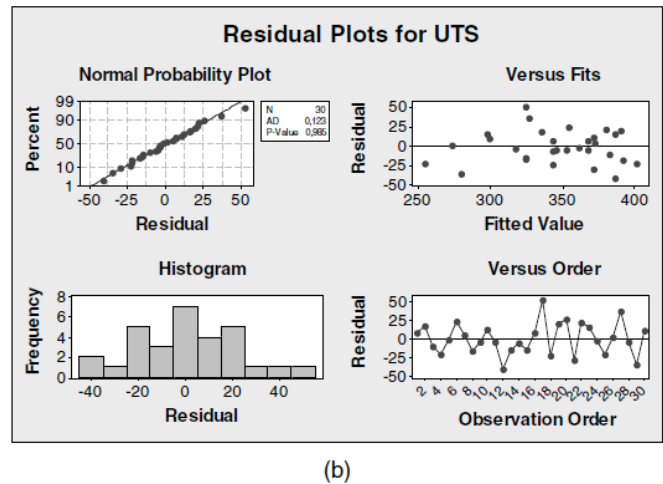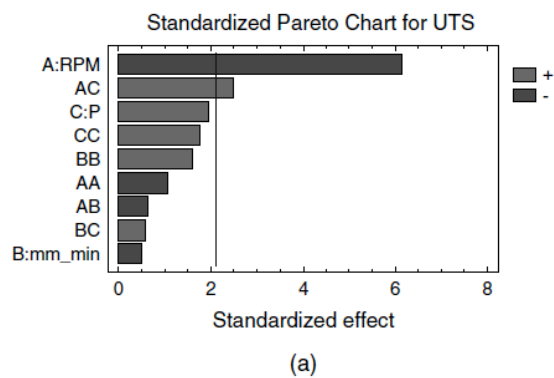
Tab. 10 ANOVA for UTS.

Fig. 18 - ANOVA of the UTS: (a) regression Pareto chart and (b) residual plot ($A = \omega$, $B = v_a$, and $C = p$).
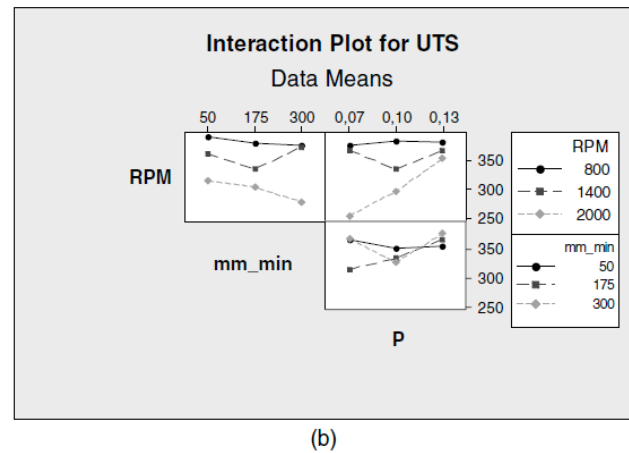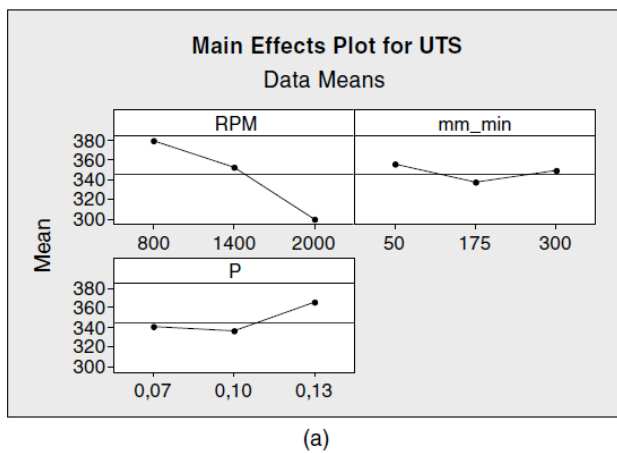

Fig. 19 - ANOVA of the UTS: (a) main effect and (b) interaction plot.

Optimizing different parameters at the same time (i.e. UTS and YS) in these conditions is then really a critical issue. The challenge is to find something able to act as a compromise between the maximum values of both mechanical properties (i.e. something that simultaneously brings both the UTS and YS at highest possible values), even if each of them does not reach the optimum value. It is so possible to introduce a *Desirability* function. This is a special function that serves to turn multiple response optimization problems into single-response problems. The first step consists in considering all measured values of a property and attributing them a numerical value ranging from 1, attributed to the lowest measured value, up to 3, attributed to the highest measured value. Obviously, a linear interpolation is made for all measured values falling between the minimum and the maximum value. In this case this is made, of course, for both UTS and YS. Therefore, each specimen, identified by a set of process parameters, is characterized by two numerical values (the former associated with UTS and the latter associated with YS). The second step consists in calculating the product of these two values. The greatest of these values corresponds to the *desired* best compromise of process parameters. Note that only welding and angular speed have been considered as variables; plunging depth has been considered as a constant, since best performances are always achieved for its maximum value. Table 9 shows the values attained by the parameters to achieve the best possible compromise. The comparison of these values with the optimum ones provided in

Table 11, allows appreciating how close they are. Figure 23 shows the spatial representation of the adopted *Desirability* function. In conclusion, the weld pitch does not seem to be a parameter able to characterize the technique under investigation. Both the YS and the UTS vary with different trends covering the angular speed *(ω)*, its square *(ω²)* and its interaction with the plunging depth *(ω · p)*. The welding speed *(va)* appears in the YS model solely in order to optimize it, but it is not a factor that significantly influences the performance. The best conditions are achieved with high weld pitch (cold joint) and high plunging depth.

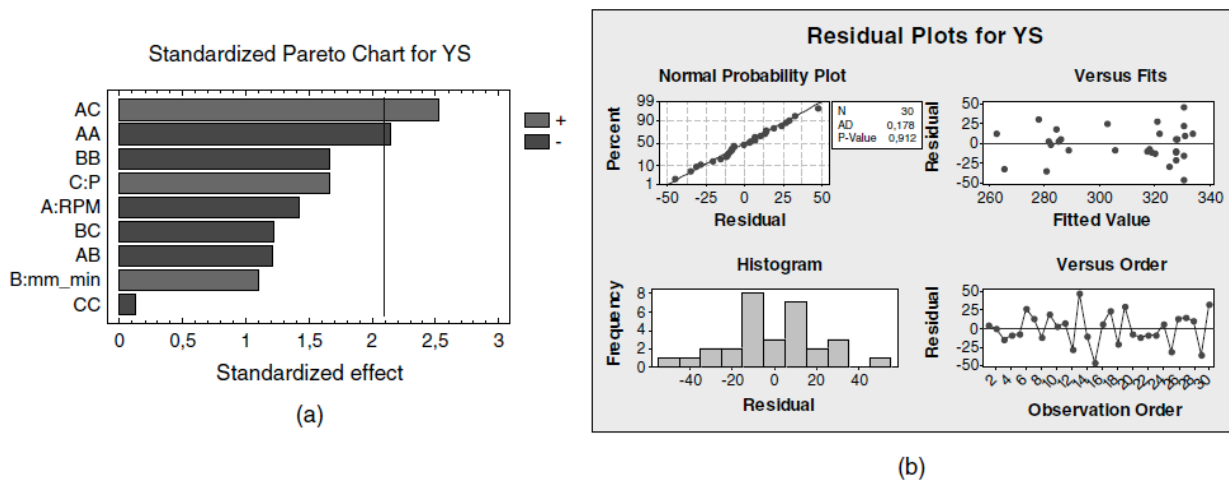| Optimize desiderabiliy			
Factor	*Low*	*High*	*Optimum*
ω [RPM]	800	2000	800
v_a [mm/min]	50	300	295
p [mm]	0.07	0.13	0.07
Response	Optimum	Base Material	Maximum
YS [MPa]	342	402	342
UTS [MPa]	403	451	410

Tab. 11 Optimal conditions for YS and UTS.

(a)

(b)

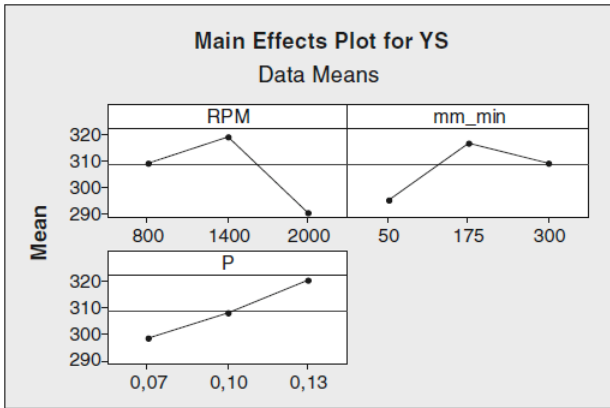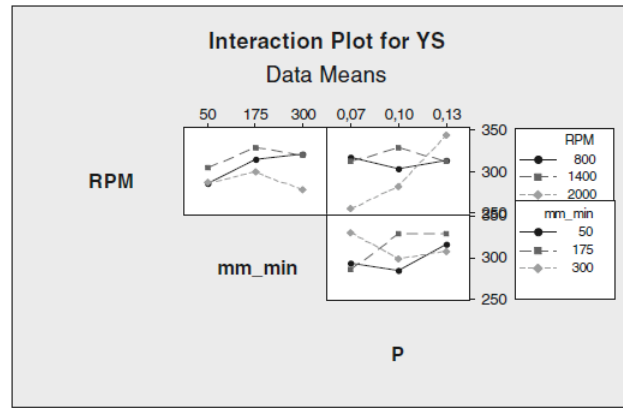*Fig. 20 - ANOVA of YS: (a) regression pareto chat and (b) residual plot (A = **ω**, B = va, and C = p)*

Fig. 21 - ANOVA of the YS: (a) main effect and (b) interaction plot.

	Maximize UTS		
Factor	**Low**	**High**	**Optimum**
ω [RPM]	800	2000	800
v_a [mm/min]	50	300	295
p [mm]	0.07	0.13	0.07
	Maximize YS		
ω [RPM]	800	2000	1650
v_a [mm/min]	50	300	50
p [mm]	0.07	0.13	0.13

Tab. 12 - Maximum conditions for UTS and YS.
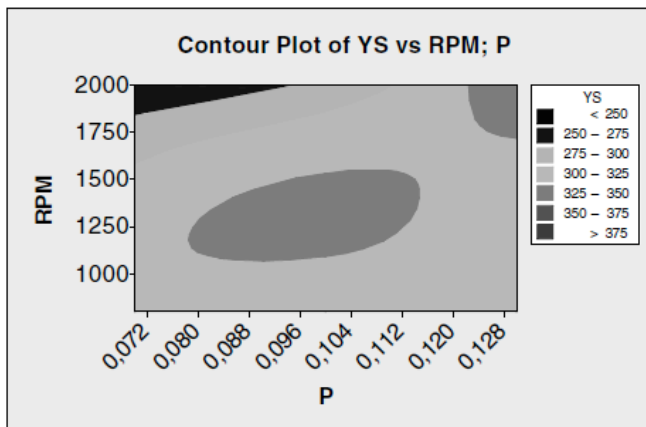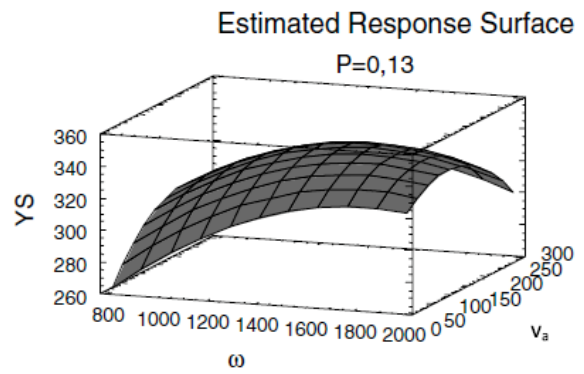
Fig. 22 - Model of YS: (a) contour plot and (b) estimated response surface.
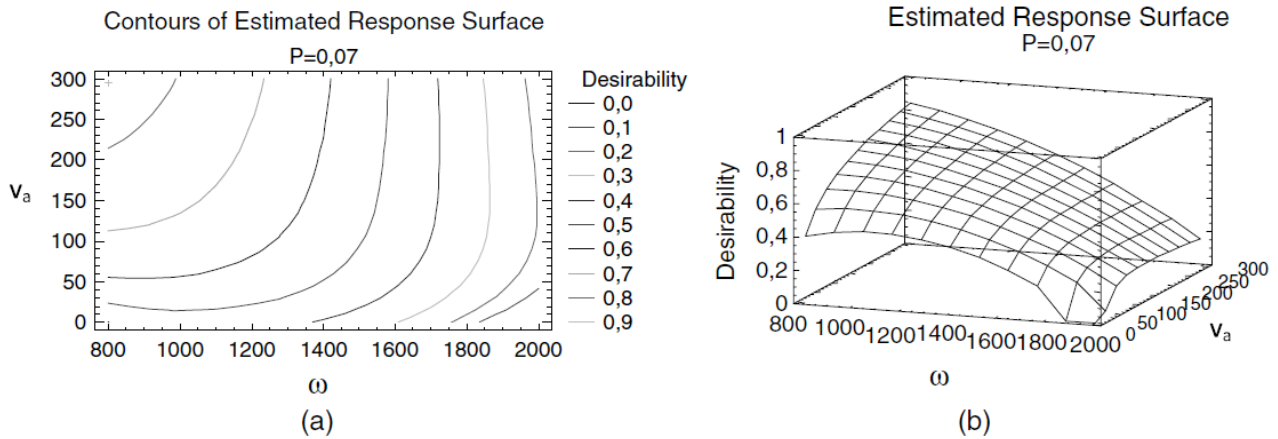
Fig. 23 - Optimal conditions for UTS and YS: (a) contours plot and (b) estimate response surface.

	Factors			Results	
Sample	N [RPM]	V [mm / min]	Position [mm]	YS [MPa]	UTS [MPa]
1	1400	175	0.10	/	/
2	800	300	0.10	307	374
3	2000	175	0.13	280	300
4	800	175	0.13	329	403
5	1400	175	0.10	317	337
6	1400	175	0.10	/	/
7	1400	300	0.13	308	412
8	1400	175	0.10	/	/
9	2000	175	0.07	275	290
10	1400	50	0.07	284	412
11	800	50	0.10	281	403
12	2000	50	0.10	292	314
13	1400	50	0.13	297	346
14	800	175	0.07	319	379
15	2000	300	0.10	310	369
16	1400	300	0.07	311	380

Tab. 13 - Resume of tensile tests.

5.1.2-c Microstructure

The defect analysis highlighted the tendency to form the tunnel defect in the welds characterized by lower weld pitch values, while the kissing bond defect occurrence is related to the plunging depth. The comparison of the defect analysis with the tensile test results allowed recognizing the influence of each defect on the joint strength. The highest values of the weld pitch allowed to obtain the best strength results, furthermore, the absence of kissing bond led to the best tensile results attained by the joints n. 10 and n.7 as summarized in Table 13. In the following pictures there are the micrographic analysis results for the best and the worst joints, respectively, identified as the BX1 and AY1 joints. The mean grain dimension mapping comparison highlighted that the lower the weld pitch the lower the extension of the NZ and the higher the extension of the HAZ (Figs 23 and 24, Tables 14 and 15). This justifies the reduction of the joints strength. The softening trend is visualized in the micro-hardness profiles (see Figs 25 and 26); in the two figures, each curve represents a hardness profile of cross section of the joint at a different depth,

according to the grid reported in Fig. 10. The grids of the micro-hardness measurements and the hardness profiles for the best and the worst UTS joints are reported in Tables 14 and 15, and respectively. Low weld pitch values result in low micro-hardness values. The micro-hardness profiles for the best sample exhibit the lowest values in the TMAZ region. The increasing of the friction heat transfer induces a diffuse decay of mechanical properties in joint and tends to develop large defects. The mean grain dimension measurements highlighted that the lower the weld pitch the lower the grain size within the NZ. The others weld regions, in terms of mean grain dimension, are less sensitive to the weld pitch.
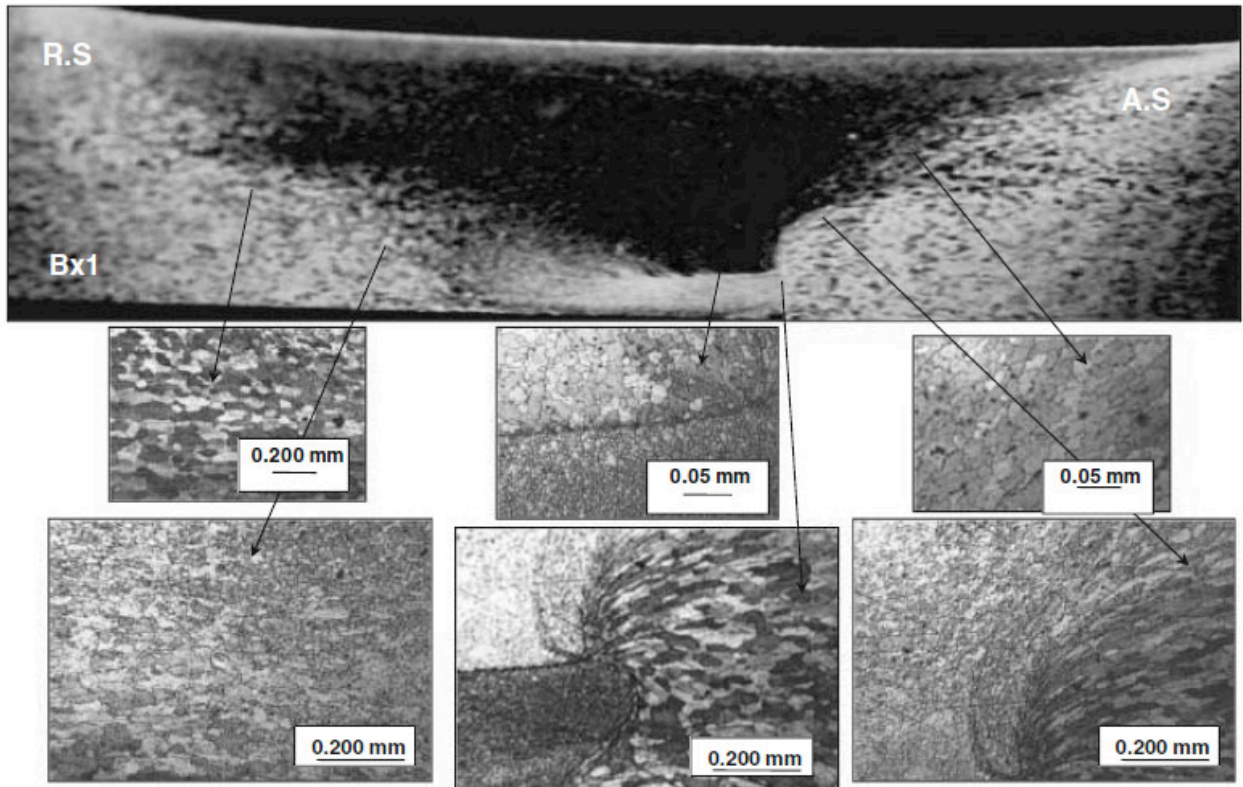

Fig. 23 - Macro and micro-structural analysis of the best UTS joint.

Mean grain dimension (μm) BX1

48.3	43.5	35.8	13.0	10.2	11.0	9.6	12.5	9.6	11.4	16.8	28.0	48.2
40.6	50.5	43.5	28.8	14.6	13.9	12.5	13.8	14.1	12.5	33.6	52.6	35.4
40.4	47.8	44.8	40.6	33.9	13.0	7.9	12.5	11.0	38.4	44.5	49.6	43.7
50.3	47.6	53.2	42.9	39.4	11.9	10.6	11.5	14.9	47.0	<u>54.8</u>	46.6	44.2
45.2	43.9	48.0	45.4	39.5	23.3	10.0	8.4	<u>6.6</u>	45.2	44.8	48.0	48.5

Standard deviation of the mean grain dimension

15.9	16.9	26.4	8.6	7.2	6.6	4.9	7.9	<u>4.1</u>	5.7	12.0	20.4	25.0
18.9	23.6	18.2	39.8	8.1	7.4	9.3	4.3	5.5	5.8	18.8	20.4	18.2
19.2	17.3	18.9	25.6	29.5	5.1	4.2	4.3	5.0	25.5	10.8	20.5	21.2
22.6	27.1	<u>42.2</u>	15.0	25.7	5.9	4.2	4.6	9.4	14.9	32.0	21.2	15.5
18.9	16.5	26.6	21.9	14.1	18.1	5.4	6.7	5.9	19.7	20.5	21.1	19.1

Tab. 14 - Grids of mean grain dimension measurements and standard deviation of mean grain dimension of the best UTS joint.

Mean grain dimension, AY1 (μ m)

44.30	35.10	24.60	12.00	8.10	10.80	10.20	7.35	10.30	27.35	46.90	32.80	41.00
44.40	39.60	41.10	24.60	26.50	9.20	8.00	7.10	17.90	45.10	39.95	40.60	44.15
59.15	46.55	55.85	31.20	15.80	7.10	7.00	8.60	23.30	36.10	34.30	35.80	48.90
44.00	36.10	46.00	43.40	24.50	7.10	4.70	4.70	22.20	37.00	39.85	47.80	44.80
39.90	45.10	44.00	30.60	42.30	20.15	5.60	4.90	34.10	26.10	47.85	48.45	42.45

Standard deviation of the mean grain dimension

21.64	21.77	27.15	7.27	3.94	4.78	3.40	3.28	3.23	24.28	30.62	22.34	13.12
13.30	32.30	40.75	34.13	29.53	5.17	3.74	3.83	13.61	22.13	25.35	15.97	28.59
23.55	21.24	24.49	23.68	17.21	4.66	3.39	3.63	26.50	21.30	12.84	16.58	7.30
4.83	14.18	32.07	23.71	23.74	3.58	1.52	2.36	21.39	11.72	26.02	6.81	12.28
11.62	24.99	16.38	15.19	25.11	15.26	2.38	2.27	14.08	19.37	14.54	15.14	17.66

Tab. 15 - Grids of mean grain dimension measurements and standard deviation of mean grain dimension of the worst UTS joint.
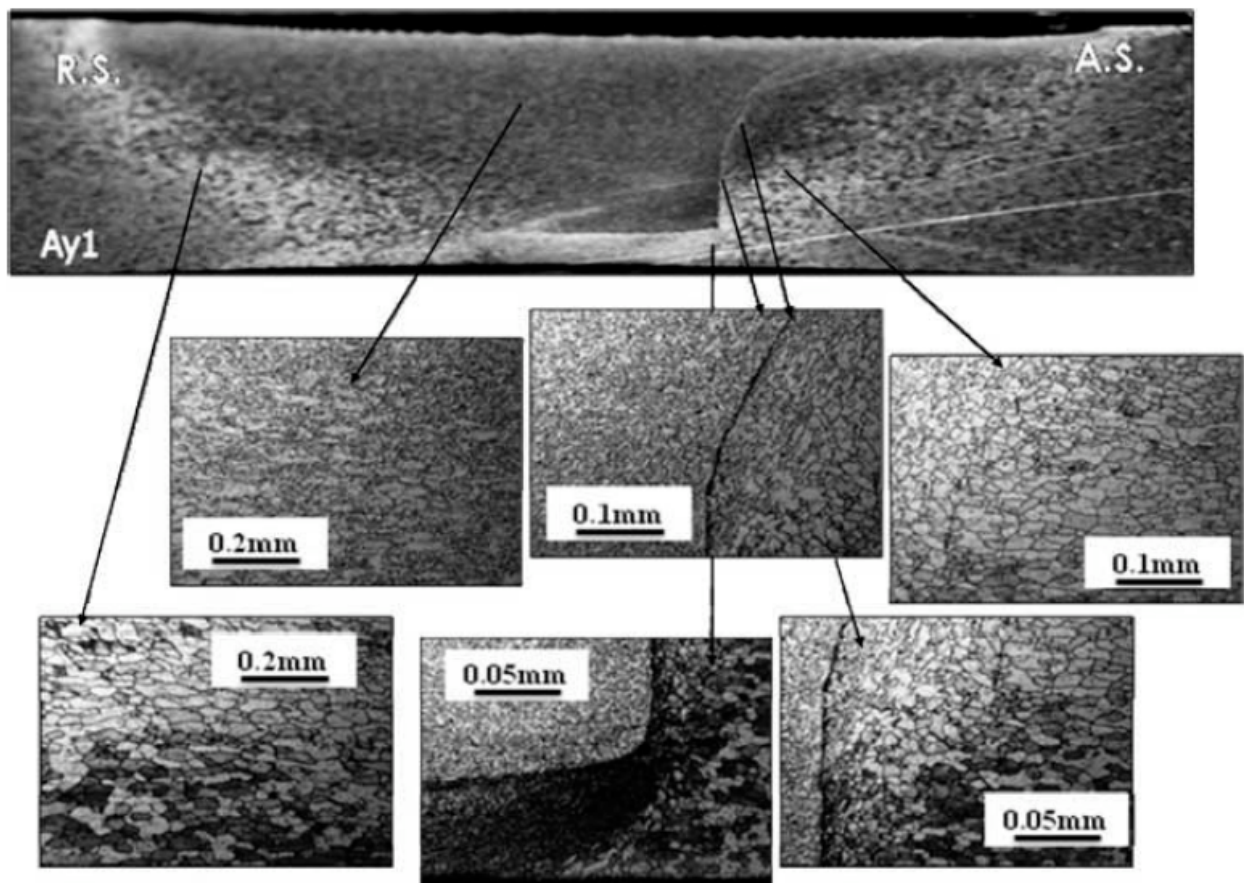

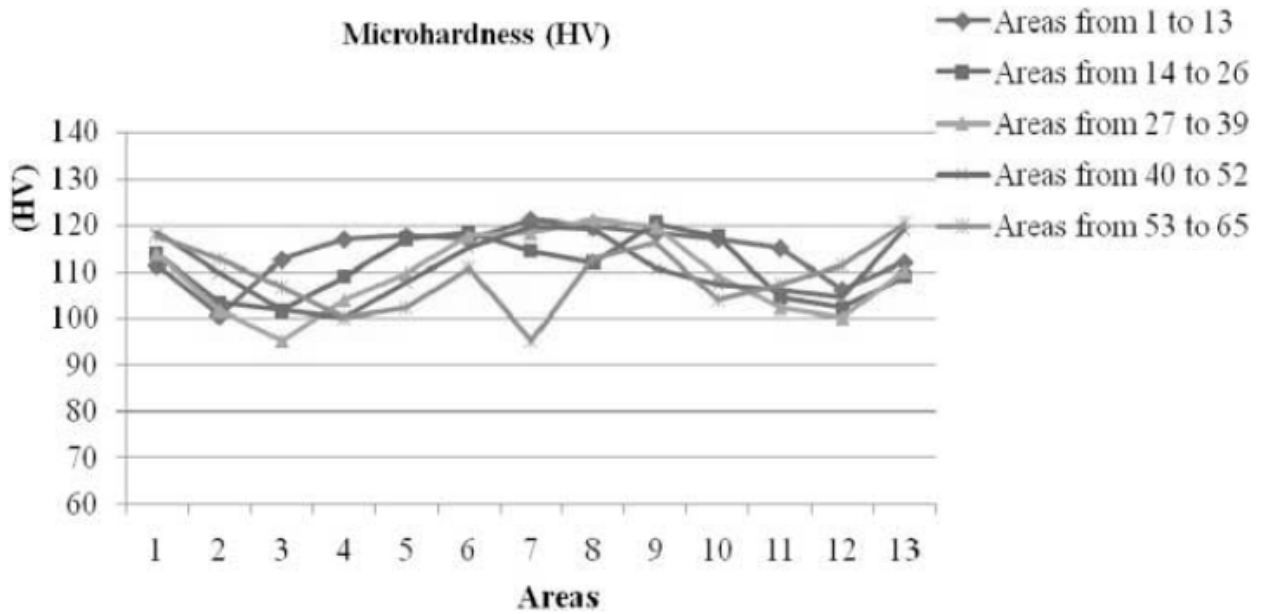fig. 24 Macro and micro-structural analysis of the best UTS joint.

fig. 25 Micro-hardness trend of the best UTS joint at different depths from the top weld
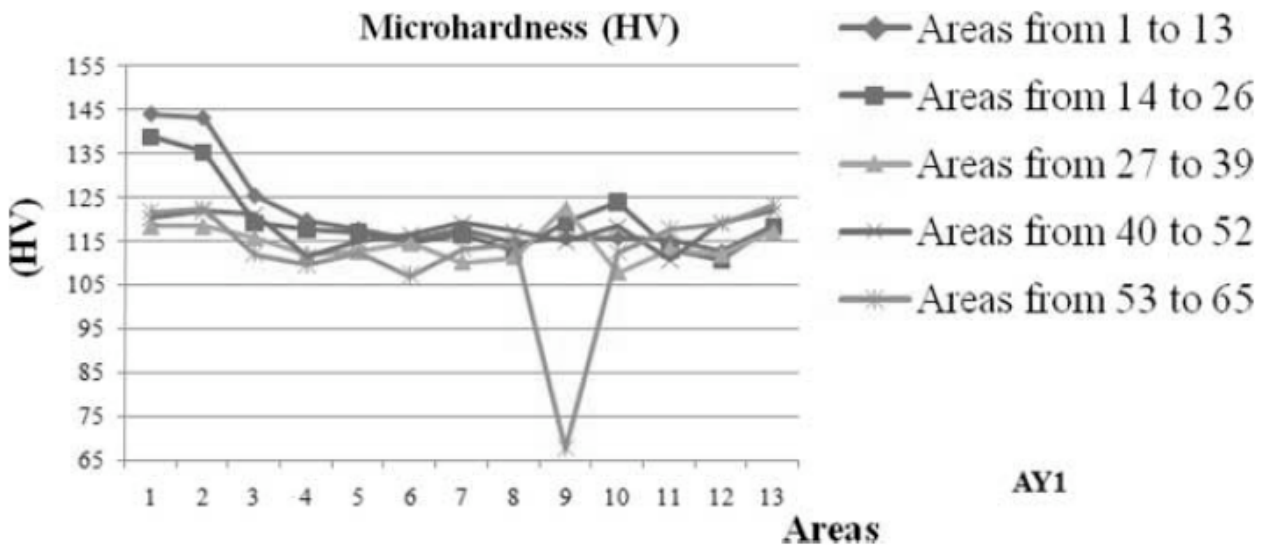

fig. 26 Micro-hardness trend of the worst UTS joint at different depths from the top weld.

5.2 AA 2198 T351

As for the AA 21239 T851, the Design of Experiment technique was used to obtain information about the influence of different process parameters on mechanical characteristics of joints and to determine the best parameters combination to improve mechanical performance at the same time.

A full factorial 3^3 scheme with 4 times replied central point was realized. Process parameters were: tilt angle, plunge thickness, rotational speed, welding rate and the relative position of the specimens to run-in. The first two were fix factors, were set at 2° and 0.1 mm respectively. The rotational speed and welding rate were classified as range value, as are variable factors. Furthermore, in this case the aim was also to verify that the weld is characterized by uniform properties in its length, in order to check if the process has reached a stationary state. Because of it, it was decided to analyze a third parameter, that was called "Position", which considers the relative position of the specimens on the joint carried out. Position at level 1 is referred to specimens in the run-in side, level 3 is referred to specimens in the run-out side, level 2 is a central place on the joint. The two welding plates were fixed on machining board (fig. 27), the working parameters were set in input to a part program as experimental plan. Sensor force signal acquisition software and part program started at the same time.
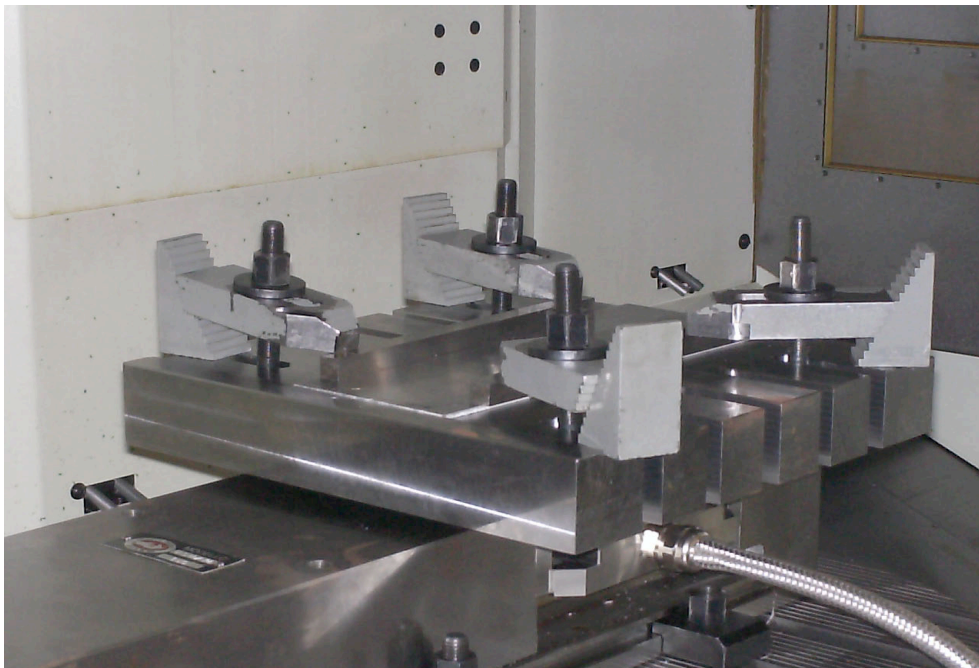

fig. 27 Welding plates blocked on the working board.

Position	Level	-1	0	1
	Value	1	2	3
Rotational Speed ω, RPM	Level	-1	0	1
	Value	500	700	900
Welding rate Va, mm/min	Level	-1	0	1
	Value	150	225	300

Tab. 16 Experimental set of parameters for AA 2198 T351.

5.2.1 Obtained results.

<u>5.2.1-a. Forces.</u>

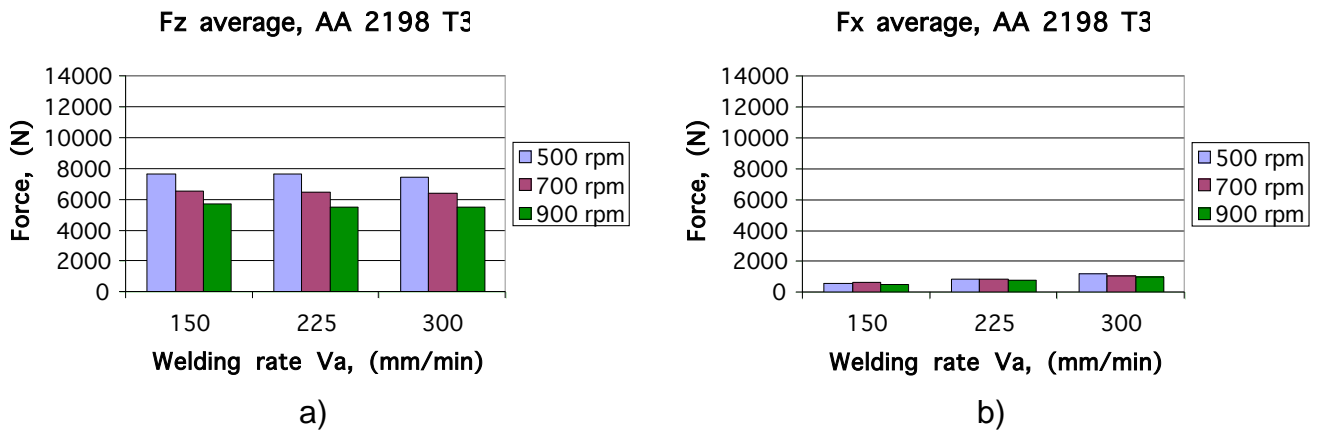a)   b)

Fig. 28 – Trend of Fz and Fx (in regime conditions) to vary the ω and Va

In Fig.28-a there was a reduction of Fz when raise the rotational speed, and so even lowest evidence with increasing the welding rate. For Fx this gap is not as marked (Fig.28-b), the trends relative to the characteristics speed of the process, is less obvious and clear.

Analysis of Variance for F med

Source	DF	Seq SS	Adj SS	Adj MS	F	P
Regression	5	6181592	6181592	1236318	28,38	0,000
Linear	2	5802246	5802246	2901123	66,6	0,000
Square	2	372219	372219	186110	4,27	0,070
Interaction	1	7126	7126	7126	0,16	0,700
Residual Error	6	261358	261358	43560		
Lack-of-Fit	3	109647	109647	36549	0,72	0,602
Pure Error	3	151711	151711	50570		
Total	11	6442949				

S = 208,710   PRESS = 1333103
R-Sq = 95,94% R-Sq(pred) = 79,31% R-Sq(adj) = 92,56%

Tab.17 Anova of the Fz medium value at regime conditions

The made it DoE, allows to perform the analysis of variance (Anova) of the factors of interest. The result holds for the Fz are shown in Tab.17, it appears that the linear terms have a high importance (99,99% reliability) and the square terms (93%) are just a little less important, in fact ω and Va, to have a dominant effect on progress of Fz (with a reliability equal to 99.99%), also must be considered the square of rotational speed (96% reliability), the square of welding rate is negligible. The Lack of Fit with P-value = 0.602, ensures that the deviation from the real system is negligible and only due to error of measurement.
Removing non-significant factors, we obtain the model shown in Table 18, which shows an R^2 = 94.15%.

Regression Analysis: F med versus N; va; N2
The regression equation is
F med = 5953 + 8,72 N + 9,17 va - 0,00874 N^2

Predictor	Coef	SE Coef	T	P	VIF
Constant	5953	1304	4,56	0,002	
N	8,718	3,76	2,32	0,049	99
va	9,169	1,008	9,1	0	1
N2	-0,008738	0,00267	-3,27	0,011	99

Analysis of Variance

Source	DF	SS	MS	F	P
Regression	3	6168735	2056245	59,99	0,000
Residual Error	8	274214	34277		
Lack of Fit	5	122503	24501	0,48	0,776
Pure Error	3	151711	50570		
Total	11	6442949			

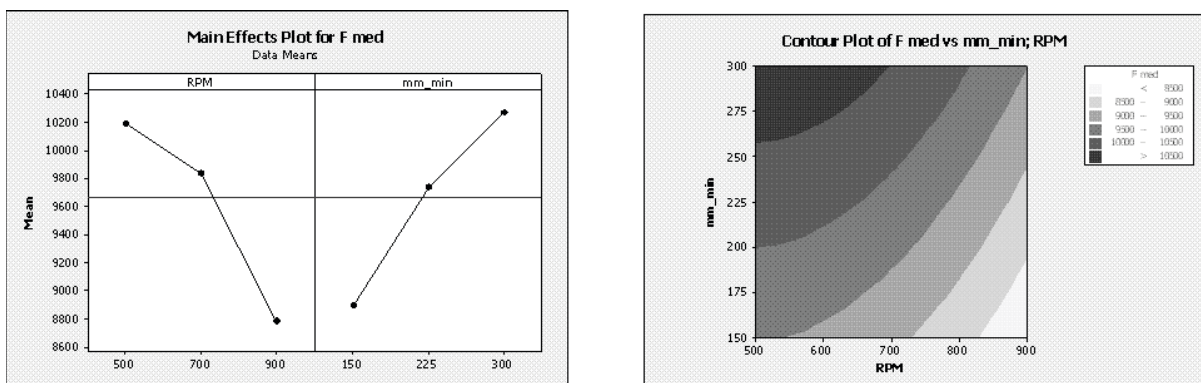Tab.18 Anova of the Fz medium value at regime conditions, optimum model

Fig. 29 – Main Effect Plot and Contour Plot of Fz model

The Main Effect plot provide a clear indication of the influence of process parameters, such as the Contour plot (Fig.29), which shows that the highest Fz occur by performing a welding with low rotational speed and high welding rate, the conditions that characterize the cold joints. Not significant interactions were revealed by ANOVA.
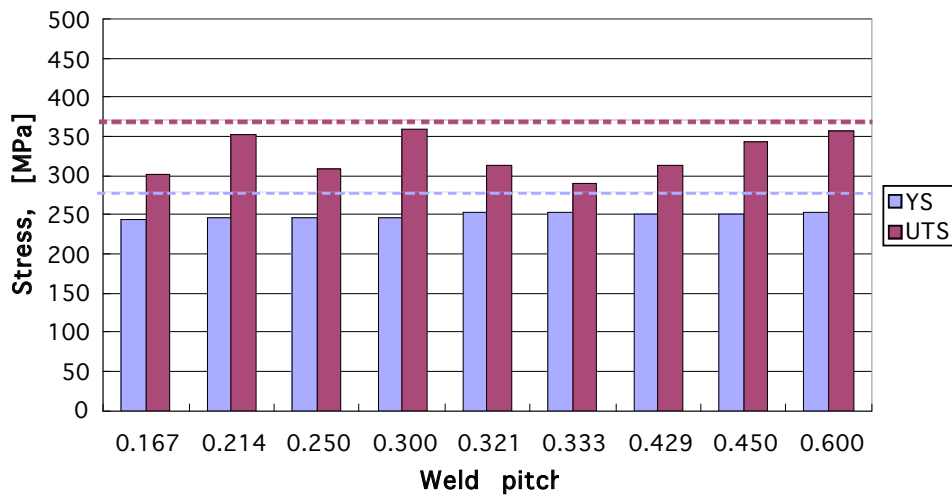
5.2.1-b Mechanical properties

Fig. 30 – YS, UTS vs weld pitch for AA 2198 T351

The tensile tests have performed the results shown in Fig.3, YS and UTS are shown vs Weld Pitch, defined as Va / ω, the dotted lines represent the values assumed by the parent alloy. The absolute values of YS and UTS are lower than other AA 2xxx series, but they are all much closer to the values found for the parent alloy, then, as will be explained below, we obtain a greater recovery of the property of the alloy (>90%), and this results in a higher performance. For the YS, is possible to observe an almost constant trend to vary the ratio of weld pitch, while the UTS is not characterized by particular trends. Furthermore, there was a decrease of the UTS to increase the rotational speed, while the YS is not characterized by pattern trends.
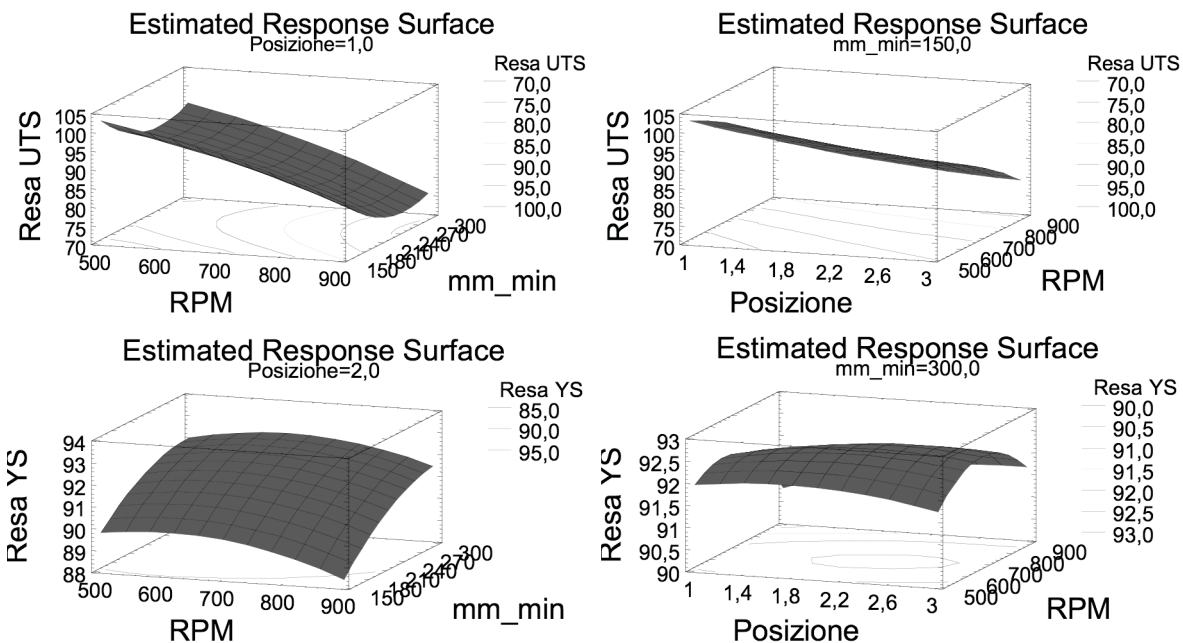

Fig.31 – Performance of YS and UTS

The maximum performance of UTS and YS (Fig.31), do not achieve at the same condition of the parameter. Indeed, the UTS reaches the maximum when the rotational speed and the welding rate are slowest (respectively ω=500 rpm, Va=150 mm/min), and the specimen

is placed near the run-in (Position=1). Instead, the maximum of YS is reached at highest weld rate (va=300 mm/min), rotational speed (ω=700 rpm) and Position (Position=2) at medium values. For effect of these observations, this parameter is practically irrelevant.

Then it was possible to proceed with the analysis of mechanical properties through the technique of ANOVA. An investigation about UTS (Tab.19), shows a greater influence of the rotational (ω) and welding (va) rate. In a regression analysis carried out (Fig.5-b), we can understand that are dominant the effects induced by rotational speed, while va can be neglected, since the influence on the UTS is in a reduced amount than the previous. On the contrary, the quadratic trend (Va^2) induced by the welding rate is important. In addition the factor Position, as Va, does not affect significantly the UTS. Interactions between parameters are not appreciable. The influence of main parameters is reported in Fig.32-a, it is clear that the variance induced by the N is much higher than the one detected by other factors.

Analysis of Variance for UTS, using Adjusted SS for Tests

Source	DF	Seq SS	Adj SS	Adj MS	F	P
Position	2	935,4	132,1	66	0,24	0,793
N	2	19470,3	19762	9881	35,71	0,000
Va	2	4362,6	4118,8	2059,4	7,44	0,012
Position*N	4	2205,8	1627,8	406,9	1,47	0,289
Position*Va	4	2018,5	2078	519,5	1,88	0,199
N*va	4	1139,1	1139,1	284,8	1,03	0,443
Position*N*Va	8	3705,8	3705,8	463,2	1,67	0,229
Error	9	2490,2	2490,2	276,7		
Total	35	36327,7				

S = 16,6339 R-Sq = 93,15% R-Sq(adj) = 73,34%

Tab19 – Anova for UTS
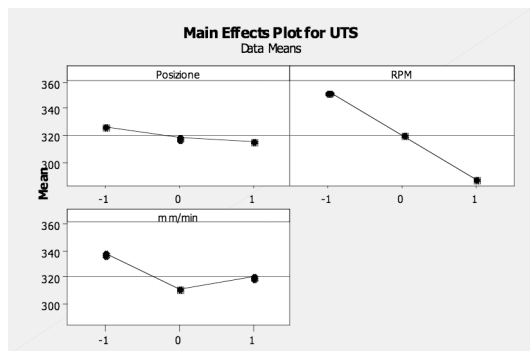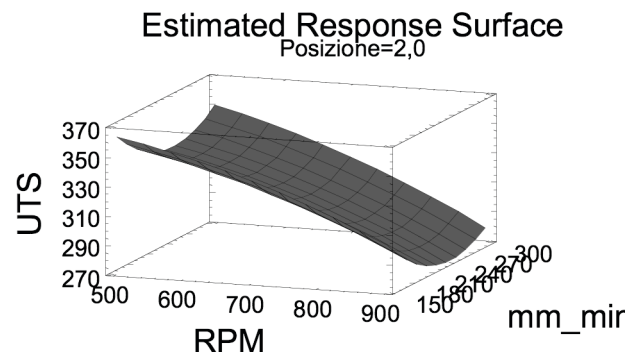
Fig.32 – UTS Anova: a)Main Effect Plot, b)Estimated Response Surface

On observe that on achieve the highest values of the UTS at low N and low Va, near the run-in (Position=1). Then, to proceeding an optimization of the regression model, on reached a numeric expression containing the factors of greatest influence of the system:

$$UTS = 565 + 1.62v_a - 0.000118\omega^2 - 0.00334v_a^2$$

The ANOVA conducted on yield strength (Tab.20), want to emphasize that all parameters, except the Position, are important for estimating of the UTS, linear and non-linear. A regression analysis carried out (Fig. 33-b), shows a high influence of welding rate (Va), the rotational speed has a reliability less than 95%, but by removing the irrelevant terms from

regression model, are likely to emerge more effectively. The influence of the Position factor is completely absent as indicated by Anova. The Main Effect plot (Fig. 33-a), while confirming the Anova analysis, shows a predominant influence of Va, and is possible to see a trend just visible of the second order of ω.

Analysis of Variance for UTS, using Adjusted SS for Tests

Source	DF	Seq SS	Adj SS	Adj MS	F	P
Position	2	3,722	6,126	3,063	2,04	0,186
N	2	90,778	40,022	20,011	13,34	0,002
Va	2	268,403	251,611	125,806	83,87	0,000
Position*N	4	49,722	51,144	12,786	8,52	0,004
Position*va	4	18,139	29,922	7,481	4,99	0,021
N*va	4	87,708	87,708	21,927	14,62	0,001
Position*N*va	8	51,917	51,917	6,49	4,33	0,021
Error	9	13,5	13,5	1,5		
Total	35	583,889				

S = 1,22474   R-Sq = 97,69%   R-Sq(adj) = 91,01%

Tab 20 – Anova for YS
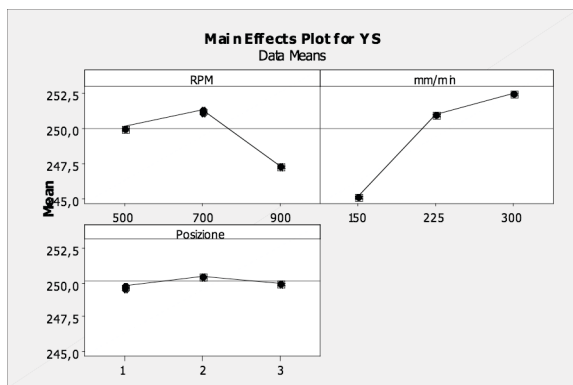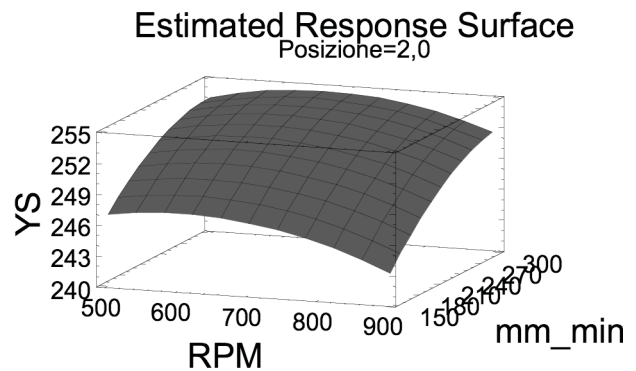
a)   b)

Fig.33 – YS Anova: a) Main Effect Plot, b) Estimate Response Surface

Through the representation of the response surface (Fig. 33-b), we see that with the experimental plan realized are unable to locate a maximum on the YS, which is achieved by using intermediate values of the velocity characteristics of the tool welding and intermediate position between run-in and run-out. In this case, the numerical optimization of the model led to the following expression:

$$YS = 214 + 0.0828\omega + 0.0496v_a - 0.0000639\omega^2 - 0.00334v_a^2$$

The ANOVA analysis has shown that the conditions in which it is possible to achieve the maximum UTS does not match with those that allow to reach the maximum of YS. The above mentioned data are summarized in the Table 21. Optimizing parameters in these conditions is really a critical issue. At this point the challenge could be the necessity to find something able to act as a compromise between the maximum values of both mechanical properties, something that simultaneously makes both the UTS and YS at highest possible values, while not reaching each of their optimum value. It's so possible to introduce a *Desiderability* function that allows to turn multiple response optimization problems into single response problems.

The first step consists in considering all measured values of a property, for example the UTS, and attributing them a numerical value ranging from 1, attributed to the lowest measured value, up to 3, attributed to the highest measured value. Obviously, a linear interpolation is made for all measured values falling between the minimum and the maximum value. This is made, of course, for both UTS and YS. At this time each specimen, identified by a set of process parameters, is characterized by two numerical values (the former associated to UTS and the latter associated to YS). The second step consists of calculating the product of these two values. The greatest of these values correspond to the *desired* best compromise of process parameters. Note that only welding and rotational speed have been considered as variables; plunging depth has been considered as a constant, since best performances are achieved always for its maximum value. Table 22 shows the values assumed by the parameters to achieve the best possible compromise. The comparison of these values with the optimum ones provided in Table 9, allows to appreciate how close they are. Fig.34 shows the spatial representation of the adopted *Desiderability* function.

Goal: maximize UTS
Optimum value = **380,712**

Factor	Low	High	Optimum
N, [RPM]	500,0	900,0	**500,0**
Va, [mm/min]	150,0	300,0	**150,0**
Position, [mm]	1	3	**1**

Goal: maximize YS
Optimum value = **254,574**

Factor	Low	High	Optimum
N, [RPM]	800,0	2000,0	**671,8**
Va, [mm/min]	50,0	300,0	**300,0**
Position, [mm]	0,07	0,13	**2,2**

Tab.21 – Conditions of maximum, respectively for UTS and YS

Optimize desiderability

Factor	Low	High	Optimum
N, [RPM]	500,0	900,0	**500**
Va, [mm/min]	150,0	300,0	**300**
P, [mm]	1	3	**1**

Response	Optimum	Base mat.	Max
UTS, [MPa]	**354,221**	370	380,7
YS, [MPa]	**252,847**	275	254,6

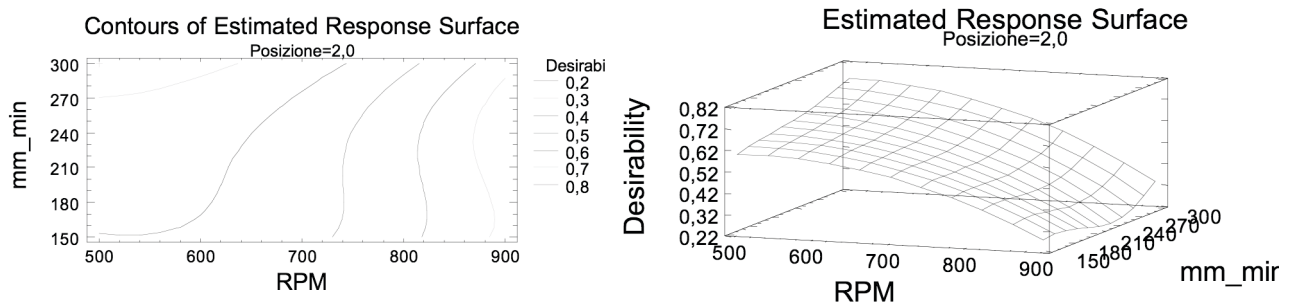Tab.22 – Optimal conditions for UTS and YS

Fig.34 – Optimal conditions for UTS and YS: Contours plot and Estimate Response Surface

In conclusion, the weld pitch is not a parameter able to characterize the system, the YS and the UTS vary with different trends that cover the rotational speed and the welding rate, and their nonlinear term. However, these parameters do not influence the same way the mechanical properties. The optimum conditions are achieved with high weld pitch (Cold Junction: N = 500rpm and Va = 300mm/min), numerically is preferable to operate in the

vicinity of the run-in (1 position), in reality this parameter does not significantly influence the process.

In order to complete the characterization carried through the tensile test, we proceed to analyze the elongation A%. Average values of A% are specified in Tab.23. The ANOVA reported in Tab.24, shows a great influence of rotational speed ω and the interaction between the Position and others parameters. Less influential, but that the Position and other interaction terms are not negligible. A regression analysis, showed that A% is influenced by the rotational speed ω (reliability =99.99%), and its quadratic term ω^2 (97.9%). From the Main Effect Plot shows clearly the effect of N, A% assumes maximum values at low rotational speed (A% ≈ 10%), and in these conditions are made more ductile joints.

		N, RPM		
		500	**700**	**900**
	150	11	7,3	3,1
v, mm/min	**225**	9,2	3,9	4
	300	9,9	3,9	2,3

Tab. 23 – Average value of A%

Analysis of Variance for UTS, using Adjusted SS for Tests

Source	DF	Seq SS	Adj SS	Adj MS	F	P
Position	2	17,993	10,532	5,266	4,76	0,039
N	2	256,56	232,333	116,167	105,1	0,000
Va	2	20,366	16,702	8,351	7,56	0,012
Position*N	4	2,151	2,152	0,538	0,49	0,746
Position*va	4	46,97	59,314	14,828	13,42	0,001
N*va	4	19,039	19,039	4,76	4,31	0,032
Position*N*va	8	55,918	55,918	6,99	6,32	0,006
Error	9	9,947	9,947	1,105		
Total	35	428,944				

S = 1,05131   R-Sq = 97,68%   R-Sq(adj) = 90,98%

Tab.24 – Anova for A%
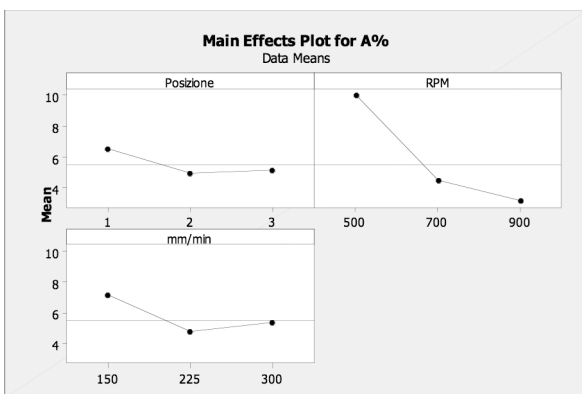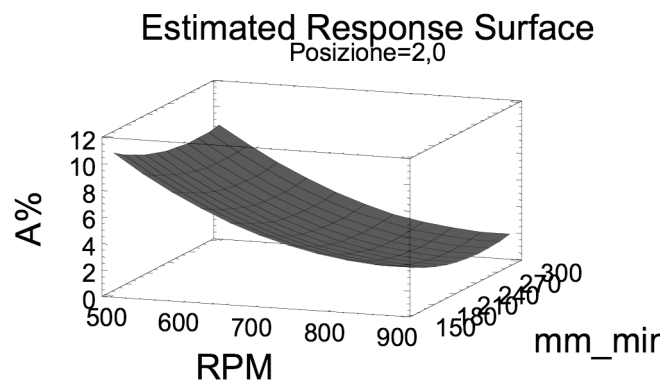
a)   b)

Fig. 35 – A% Anova: a) Main Effect Plot, b) Estimate Response Surface

A 3d representation of the model (Fig. 35-b), shows that the welding rate and the position factor are negligible compared to the rotational speed. The optimal regression model is:

$$A\% = 53,2 - 0,0931\,\omega - 0,0389\,va - 3,75\,Position + 0,000054\,\omega^2 + 0,0135\,va*Position.$$

The terms of Welding rate and Position, are necessary to optimize the model.

5.2.1-c Metallographic analysis

The study of AA 2198 T351, is comprehensive of a metallographic analysis on specimens before and after tensile tests. The aim of this analysis was to detect the presence of defects caused by welding process and, possibly, to understand how they have influence on initiation of cracking and, consequently, on the mechanical properties of the joints.
In Table 25 are reported the images related all the tested joints. In the intermediate point (ω = 700RPM and Va = 225mm/min) were carried out 4 welds, but while the breaking occurs always with the same geometry it was decided to show only one, representative for all four.
All seams do not show the presence of macroscopic defects such as tunnels, pores and Hook Defect that can weaken them. The fact that the tool is fully plunged in all the thickness of the material reduces the possibility of crack initiation induced by the non-plunging and related reduction in the useful section (Kissing Bond defect). The shape of the fracture of the joint is similar, except for the coolest one (ω = 500RPM and Va = 300mm/min) and divided in two parts: the bottom where the fracture follows the curves of material flow and a top where the material rips.

		ω [RPM]		
		500	**700**	**900**
v, [mm/min]	**150**			
	225			
	300			

Tab.25 – Samples fracture

The welding achieved in the condition of lower heat input (cold joint, N = 500RPM and Va = 300mm/min), shows a ductile fracture, characteristic of non-welded metals. In fact, it is at this combination of parameters that gives the best mechanical properties (YS and UTS), achieving a recovery of the properties of the material above the 90%.

5.2.1-d Micro-hardness

After the micrographic analysis, Vickers micro hardness (HV) measurements were carried out in the welded zone, making three lines of 50 indentations each. In this way it has been possible to subdivide the data for the five different characteristic zone of FSW, in order to evaluate the mean micro-hardness for all the sets of process parameters. A very small TMAZ has lead to the   impossibility to show any point for some welds. The results are show briefly in Tab. 26.

HAZ A				TMAZ A		
	150	225	300		150	225	300
500	87,13	86,93	88,5	**500**	89	85	101
700	89,57	87,67	93,5	**700**	81	85,5	98
900	84,5	85,19	78,73	**900**	84	88	

a)   b)

NUGGET				TMAZ R		
	150	225	300		150	225	300
500	87,53	89,93	102,14	**500**		91	
700	79,29	86,62	101,53	**700**	81	86	104,5
900	85,5	86,47	88,87	**900**	84,5	86	

c)   d)

HAZ R		
	150	225	300
500	86,06	88	90,71
700	84,52	86,64	96,75
900	87,88	88,24	88,82

e)
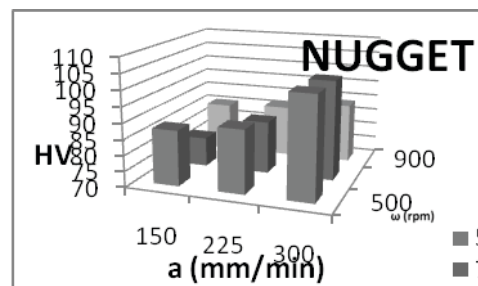
f)

Tab. 26 – Micro-hardness in a) HAZ A, b) TMAZ A, c-f) NUGGET, d) TMAZ R, e) HAZ R

Since the breaking always happens in the Nugget zone, it was decided to focus the study on the values of micro-hardness measured in that zone (Tab.26-f). The 3d histogram illustrates a greater growth of HV, when the welding rate Va is high and simultaneously the rotational speed ω is low, they are exactly the condition of cold –joint that maximize the mechanical properties UTS and YS.
The HV in the Nugget-zone seems to be influenced significantly by main effect ω and Va (P-value=0,960) and in a small by non linear effects. This is shown in Tab.27. The coefficient R^2=71,19% is very high, simultaneously the Lack of Fit (P-value=0,081) just negligible, therefore it's probably that erasing the main factors from the model of regression, with its P-value too high, that indicates to don't influence so much the HV, was possible estimate with best precision the influence of non linear effects (quadratic and interaction).
A Best Subset analysis confirm that is possible to make a functional model for HV, using only the non linear terms: ω^2, va^2 and ω*va. The regression equation is

Nugget HV = 82,4 + 0,000022 N2 + 0,000522 va2 - 0,000207 ω*va

The Anova carried out on this model (Tab.16), evidence which HV is greatly influenced by va2 (P-value=0,004) and by interaction between N and va (P-value=0,039), this last indication permit of understand which the effect of main factor not is of simple addition.

Analysis of Variance for HV Nugget

Source	DF	Seq SS	Adj SS	Adj MS	F	P
Regression	5	403,28	403,277	80,6554	6,44	0,021
Linear	2	328,26	1,031	0,5156	0,04	0,960
Square	2	43,43	43,428	21,7141	1,73	0,255
Interaction	1	31,58	31,584	31,5844	2,52	0,163
Residual Error	6	75,19	75,193	12,5321		
Lack-of-Fit	3	65,01	65,013	21,671	6,39	0,081
Pure Error	3	10,18	10,18	3,3932		
Total	11	478,47				

S = 3,54007   PRESS = 686,623
R-Sq = 84,28% R-Sq(pred) = 0,00% R-Sq(adj) = 71,19%

Tab.27 – Anova of Nugget Microhardness

The coefficient R2=71,19% is very high, simultaneously the Lack of Fit (P-value=0,081) just negligible, therefore it's probable that erasing the main factors from the model of regression, whit his P-value too high, that doesn't seem to affect significantly the HV, is possible to estimate with the best precision the influence of non linear effect (quadratic and interaction).

A Best Subset analysis confirm that is possible to make a functional model for HV, using only the non linear terms: N2, va2 and N*va. Thousand on realise the maximum of R2=78,1% and the minimum of variance. The regression equation is

Nugget HV = 82,4 + 0,000022 N2 + 0,000522 va2 - 0,000207 N*va

The Anova carried out on this model (Tab.28), evidence which HV is greatly influenced by va2 (P-value=0,004) and by interaction between N and va (P-value=0,039), this last indication permits to understand that the effect of main factor is not of simple addition. A clear trend of HV-model is show in Fig.24 by Contour plot and surface plot.

Regression Analysis

Predictor	Coef	SE Coef	T	P
Constant	82,39	3,174	25,96	0
N2	0,00002218	0,000014	1,58	0,152
va2	0,0005216	0,0001333	3,91	0,004
N*va	-0,00020695	0,00008374	-2,47	0,039

Analysis of Variance

Source	DF	SS	MS	F	P
Regression	3	402,25	134,08	14,07	0,001
Residual Error	8	76,22	9,53		
Total	11	478,47			

Tab. 28 – Regression and Anova of best model

6. Conclusions

How previously exposed, this work made possible to understand how complex phenomena are related to the FSW process, and drove to the conclusions that are remarked below.

This research activity allowed determining the influence of the FSW process parameters as the welding speed **(v**a**)** , the angular speed **(ω)** , and the plunging depth **(p)** on the mechanical properties, the microstructure and the defect morphology of butt joints of the new aluminium alloy AA 2139 T8 using a statistical investigation tool as the DOE.

The ANOVA analysis has shown that the conditions for which it is possible to achieve the maximum UTS does not match with those making possible to achieve the maximum of the YS.

The weld pitch does not appear to be a parameter able to characterize the system. The YS and the UTS vary with different trends that cover the angular speed **(ω)** , its square **(ω²)** and its interaction with the plunging depth **(ω P)** . The best conditions are achieved with high weld pitch (cold joint) and high plunging depth.

The defect analysis highlighted the tendency to form the tunnel defect in the welds characterized by low weld pitch values, while the presence of Kissing Bond defect is influenced by the plunging depth. High values of the weld pitch allowed to get the best strength results and furthermore the absence of the above-mentioned defects.

The mean grain dimension mapping comparison highlighted that the lower the weld pitch the lower the extension of the NZ and the higher the extension.

The mean grain dimension measurements highlighted that the lower the weld pitch the lower the grain size within the NZ. The other weld regions, in terms of mean grain dimension, are less sensitive to the weld pitch.

The welding technique adopted, the FSW, allows achieving very high joint performances, with respect to those achievable with conventional welding techniques, for heat-treated aluminium alloys, such as the ones under investigation in the present research work.

The forces acting in the direction perpendicular to the weld (Fz), tend to decrease by increasing rotational speed ω, and less appreciably by decreasing the weld rate va.

The forces Fx, parallel to the welding direction, seem to don't undergo major variations, while the trend is an increase when the weld rate va is increased.

The UTS show a stronger dependence by rotational speed ω, and show a reverse proportionality, in fact for lower value of ω the greater values of Ultimate Tensile Strength. Moreover are achieved, and the evidence of a non linear dependence by weld rate va.

The YS, on the contrary of the UTS, depended significantly by weld rate va. In this case is possible to observe a direct proportionality, in fact to the higher va corresponds the greater yield strength, while a non linear dependence with the rotational speed ω was found.

The elongation A%, analogously to UTS, highlights a great dependence on ω, in particular the maximum elongation was found in correspondence of low rotational speeds, for the same values that maximize the UTS.

The metallographic analysis shows the absence of characteristic defects of FSW joints. All joints achieve the breakdown in the NZ, with a fracture that tends to follow the flow lines of material, except the joint produced in the cold conditions (low rotational speed ω and high weld rate va), which exhibits a ductile fracture that is characteristic of non-welded material. This weld is characterized by greater mechanical performances, showing simultaneously the best values of UTS and YS above all the joints, with a recovery up to 90% of the properties of base material.

References

[1]   Thomas, W.M. (1991) Friction Stir Welding, International Patent Application No. PCT/GB92/02203 and GB Patent Application No. 9125978.8, December, US Patent No. 5,460,317.

[2]   Mishra RS, Ma ZY. Friction stir welding and processing. Mater Sci Eng R 2005; 50(1-2): 1-78

[3]   Dawes CJ, Thomas WM. Friction stir process welds aluminum alloys. Weld J 1996; 75(3): 41-5

[4]   Fuji H, Cui L, Tsuji N, Maeda M, Nakata K, Nogi K, Friction stir welding of carbon steel. Mater Sci Eng A 2006; 429(1-2); 50-7

[5]   Hovanski Y, Santella ML, Grant GJ, Friction stir spot welding of hot stamped boron steel. Scripta Mater 2007;57(9):873-6

[6]   Sato YS, Yamanoi H, Kokawa H, Furuhara T, Microstructural evolution of ultrahigh carbon steel during friction stir welding. Scripta Mater 2007;57(6):557-60.

[7]   Ueji R, Fujii H, Cui L, Nishioka A, Kunishige K, Nogi K, Friction stir welding of ultrefine grained plain low carbon steel formed by martensite process. Mater Sci Eng A 2006;423(1-2):324-30

[8]   Lee W-B, Lee C-Y, Chang W-S, Yeon Y-M, Jung S-B. Microstructural investigation of friction stir welded pure titanium. Mater Lett 2005;59(26):3315-8.

[9]   Reynolds AP, Hood E, Tang W. Texture in friction stir welds of Time tal 21s. Scripta Mater 2005;52(6):491-4

[10]   Feng AH, Ma ZY. Enhanced mechanical properties of Mg-Al-Zn cast alloy via friction stir processing. Scripta Mater 2007; 56(5): 397-400

[11]   Xie GM, Ma ZY, Geng L, Chen RS. Microstructural evolution and mechanical properties of friction stir welded Mg-Zn-Y-Zr alloy. Mater Sci Eng A 2007; 471(1-2): 63-8

[12]   Lee W-B, Jung S-B. The joint properties of copper by friction stir welding. Mater Lett 2004; 58(6):1041-6

[13]   Sakthivel T, Mukhopadhyay J. Microstructure and mechanical properties of friction stir welded copper. J Mater Sci 2007; 42(19):8126-9

[14]   Xie GM, Ma ZY, Geng L. Development of a fine-grained microstructure and the properties of a nugget zone in friction stir welded pure copper. Scripta Mater 2007; 57(2): 73-6

[15]   Feng AH, Ma ZY, Formation of Cu2FeAl7 phase in friction-stir-welded SiCp/Al-Cu-Mg composite. Scripta Mater 2007;57(12):1113-6

[16]   Storjohann D, Barabash OM, David SA, Sklad PS, Bloom EE, Babu SS, Fusion and friction stir welding of aluminum-metal-matrix-composites. Metall Mater Trans A 2005;36(11);3237-47

[17]   Cerri E, Leo P. Warm and room temperature deformation of friction stir welded thin aluminum sheets Materials and Design 2010; 31: 1392–402

[18]   Fratini L, Pasta S, Reynolds AP. Fatigue crack growth in 2024-T351 friction stir welded joints: Longitudinal residual stress and microstructural effects. International Journal of Fatigue 2009; 31: 495–500

[19]   Golestaneh AF, Aidy A, Zadeh M. Modelling the fatigue crack growth in friction stir welded joint of 2024-T351 Al alloy. Materials and Design 2009; 30: 2928–37

[20]   Shanmuga Sundaram N, Murugan N, Dependence of ultimate tensile strength of friction stir welded AA2024-T6 aluminium alloy on friction stir welding process parameters. Mechanika 2009; 78: 17-24

[21] Jariyaboon M, Davenport AJ, Ambat R, Connolly BJ, Williams SW, Price DA. The effect of welding parameters on the corrosion behaviour of friction stir welded AA2024-T35. Corrosion Science 2007; 49: 877-909

[22] Chen CS, Yang JG, Tan AH. Study of welding peak temperatures on microstructures and hardness of heat affected zone in 2024-T3 aluminium alloy. Materials Science and Technology 2009; 25(7): 896-904

[23] Dattoma V, De Giorgi M, Nobile R. On the Residual Stress Field in the Aluminium Alloy FSW Joints. STRAIN 2009; 45(4): 380-6

[24] Cavaliere P, De Santis A, Panella F, Squillace A. Effect of welding parameters on mechanical and microstructural properties of dissimilar AA6082–AA2024 joints produced by friction stir welding. Materials and Design 2009: 30 609–16

[25] Dressler U, Biallas G, Mercado UA. Friction stir welding of titanium alloy TiAl6V4 to aluminium alloy AA2024-T3. Materials Science and Engineering A 2009; 526: 113–7

[26] Xu W, Liu J. Microstructure and pitting corrosion of friction stir welded joints in 2219-O aluminum alloy thick plate. Corrosion Science 2009; 51: 2743–51

[27] Chen YC, Feng JC, Liu HJ. Precipitate evolution in friction stir welding of 2219-T6 aluminum alloys. Materials Characterization 2009; 60: 476-81

[28] Surekha K, Murty BS, Prasad Rao K. Effect of processing parameters on the corrosion behaviour of friction stir processed AA 2219 aluminum alloy. Solid State Sciences 2009: 11 907–17

[29] Xu W, Liu J, Luan G, Dong C. Microstructure and mechanical properties of friction stir welded joints in 2219-T6 aluminum alloy. Materials and Design 2009: 30 3460–3467

[30] Hatamleh O, Mishra RS, Oliveras O. Peening effects on mechanical properties in friction stir welded AA 2195 at elevated and cryogenic temperatures. Materials and Design 2009; 30: 3165–3173

[31] Cavaliere P, Cabibbo M, Panella F, Squillace A. 2198 Al–Li plates joined by Friction Stir Welding: Mechanical and microstructural behavior. Materials and Design 2009; 30: 3622–31

[32] Cavaliere P, De Santis A, Panella F, Squillace A Effect of anisotropy on fatigue properties of 2198 Al–Li plates joined by friction stir welding. Engineering Failure Analysis 2009; 16(6): 1856-65.

[33] Chen C, Kovacevic R. Thermomechanical modelling and force analysis of friction stir welding by the finite element method. Journal Proceedings of the Institution of Mechanical Engineers, Part C: Journal of Mechanical Engineering Science 2004; 218(5): 509-19

[34] A. Prisco, F. Acerra, A. Squillace, G. Giorleo, C. Pirozzi, U. Prisco, F. Bellucci, LBW of Similar and Dissimilar Skin-Stringer Joints. Part I: Process Optimization and Mechanical Characterization, Advanced Materials Research, Vol. 38 (2008), pp 306-319.

[35] Elangovan K, Balasubramanian V, Babu S. Predicting tensile strength of friction stir welded AA6061 aluminium alloy joints by a mathematical model, Materials and Design 2009; 30: 188–93.

[36] Elangovan K, Balasubramanian V, Babu S, Balasubramanian M. Optimising Friction Stir Welding parameters to maximise tensile strength of AA6061 aluminium alloy joints. International Journal of Manufacturing Research 2008; 3: 321– 34

[37] Balasubramanian V. Relationship between base metal properties and friction stir welding process parameters, Materials Science and Engineering A 2008, 480: 397–403.

[38] Lakshminarayanan AK, Balasubramanian V. Comparison of RSM with ANN in predicting tensile strength of friction stir welded AA7039 aluminium alloy joints, Transactions of Nonferrous Metals Society of China 2009; 19: 9-18.

[39] Sarsilmaz F, Caydas U. Statistical analysis on mechanical properties of friction-stir-welded AA 1050/AA 5083 couples. Int J Manuf Technol 2009; 43: 248-55.

[40] R. R. Hocking And R. N. Leslie, Selection of the Best Subset in Regression Analysis, Technometrics, VOL. 9, No. 4, 1967.

[41] C. L. Mallows, Some Comments on C_p, Technometrics , VOL. 15, No. 4, 1973.

[42] C. L. Mallows, More Comments on C_p, Technometrics , VOL. 37, No. 4, 1995

[43] Balasubramanian, N.; Gattu, B.; Mishra, R.S., Process forces during friction stir welding of aluminium alloys, Science and Technology of Welding & Joining, Volume 14, Number 2, February 2009 , pp. 141-145(5).

[44] Montgomery, D.C. (2001) Design and Analysis of Experiments, John Wiley & Sons, New York.

[45] Harrington EJ, 1965. The desirability function. Industrial Quality Control 21, 494–498.

[46] Derringer G, Suich R. Simultaneous optimization of several response variables, Journal of Quality Technology 1980; 12: 214–219.

[47] Cavaliere, P., Campanile, G., Panella, F., and Squillace,, A. Effect of welding parameters on mechanical and microstructural properties of AA6056 joints produced by friction stir welding. J. Mater. Process. Tech., 2006,180(1–3), 263–270.

[48] Cabibbo, M., McQueen, H. J., Evangelista, E., Spigarelli, S.,Di Paola, M., and Falchero, A. Microstructure and mechanical property studies of AA6056 friction stir welded plate. Mater. Sci. Eng. A, 2007, 460–461, 86–94.

[49] Cavaliere, P., Squillace, A., and Panella, F. Effect of welding parameters on mechanical and microstructural properties of AA6082 joints produced by friction stir welding. J.Mater. Process. Technol., 2008, 200, 364–372.

[50] Genevois, C., Deschamps, A., and Vacher,P. Comparative study on local and global mechanical properties of 2024 T351, 2024 T6 and 5251 O friction stir welds. Mater. Sci. Eng. A, 2006, 415, 162–170.

Index